

1 **The unfolded protein response of the endoplasmic reticulum supports mitochondrial**  
2 **biogenesis by buffering non-imported proteins**

3

4 Katharina Knöringer<sup>1\*</sup>, Carina Groh<sup>1\*</sup>, Lena Krämer<sup>1\*</sup>, Kevin C. Stein<sup>2</sup>, Katja G. Hansen<sup>3</sup>,  
5 Johannes M. Herrmann<sup>1</sup>, Judith Frydman<sup>2,4</sup>, Felix Boos<sup>1,5#</sup>

6

7 <sup>1</sup>Cell Biology, Technische Universität Kaiserslautern, 67663 Kaiserslautern, Germany

8 <sup>2</sup>Department of Biology, Stanford University, Stanford, CA 94305, USA

9 <sup>3</sup>Department of Genetics, Blavatnik Institute, Harvard Medical School, Boston, MA 02115, USA

10 <sup>4</sup>Department of Genetics, Stanford University, Stanford, CA 94305, USA

11 <sup>5</sup>Current address: Department of Genetics, Stanford University, Stanford, CA 94305, USA

12

13 \*, K.K., C.G. and L.K. contributed equally to this work

14 #, corresponding author, [fboos@stanford.edu](mailto:fboos@stanford.edu)

15 **Abstract**

16 Almost all mitochondrial proteins are synthesized in the cytosol and subsequently targeted to  
17 mitochondria. The accumulation of non-imported precursor proteins occurring upon mitochondrial  
18 dysfunction can challenge cellular protein homeostasis. Here we show that blocking protein  
19 translocation into mitochondria results in the accumulation of mitochondrial membrane proteins at  
20 the endoplasmic reticulum, thereby triggering the unfolded protein response (UPR<sup>ER</sup>). Moreover,  
21 we find that mitochondrial membrane proteins are also routed to the ER under physiological  
22 conditions. The levels of ER-resident mitochondrial precursors is enhanced by import defects as  
23 well as metabolic stimuli that increase the expression of mitochondrial proteins. Under such  
24 conditions, the UPR<sup>ER</sup> is crucial to maintain protein homeostasis and cellular fitness. We propose  
25 the ER serves as a physiological buffer zone for those mitochondrial precursors that can't be  
26 immediately imported into mitochondria while engaging the UPR<sup>ER</sup> to adjust the ER proteostasis  
27 capacity to the extent of precursor accumulation.

28

29

## 30 **Introduction**

31 The ability of cells to maintain protein homeostasis (proteostasis) is crucial for organismal health.  
32 Imbalances in protein synthesis, targeting, folding and degradation are associated with numerous  
33 diseases and are also hallmarks of aging<sup>1-5</sup>. Cells constantly monitor their proteome to quickly  
34 sense proteotoxic perturbations and launch stress-reactive programs to restore homeostasis. Of  
35 particular importance are the compartment-specific stress responses to misfolded proteins of the  
36 cytosol and nucleus (heat shock response) as well as of the endoplasmic reticulum (unfolded protein  
37 response of the ER, UPR<sup>ER</sup>) and mitochondria (UPR<sup>mt</sup>). Via the activation of dedicated transcription  
38 factors, these pathways elevate the levels of chaperones, proteases and other quality control factors  
39 in the compartment where protein misfolding is sensed<sup>6-9</sup>.

40 When misfolded proteins accumulate in the ER, the ER membrane kinase Ire1 dimerizes,  
41 autophosphorylates and then splices the mRNA of *XBPI* (*HAC1* in yeast). This enables its efficient  
42 translation, giving rise to a potent transcription factor that induces the UPR<sup>ER</sup><sup>10</sup>. Besides increasing  
43 the expression of ER chaperones and other biogenesis factors, the UPR<sup>ER</sup> can considerably expand  
44 the ER of a cell. In yeast, the Ire1-Hac1 pathway is the only dedicated regulator of the UPR<sup>ER</sup>,  
45 while mammalian cells have two additional branches of the UPR<sup>ER</sup> that control transcription,  
46 translation and eventually apoptosis via PERK and ATF6<sup>11</sup>.

47 Cellular organelles have clearly distinct organizations and functions, yet they are no independent  
48 entities; instead, they form tight physical contacts<sup>12-14</sup> and functionally cooperate in the synthesis of  
49 proteins, lipids and metabolites<sup>15,16</sup>. Hence, they mutually influence and rely on the homeostasis of  
50 one another. In many protein folding diseases, defects in proteostasis are observed in multiple  
51 organelles at the same time, even though the primary perturbation occurs in most cases in only one  
52 compartment<sup>17,18</sup>. As a consequence, the different stress response programs need to act in concert  
53<sup>19-23</sup>. For instance, perturbations of mitochondrial proteostasis often compromise mitochondrial  
54 protein import so that non-imported precursor proteins accumulate in the cytosol<sup>19,24-26</sup>.  
55 Consequently, mitochondrial dysfunction not only activates mitochondrial quality control pathways,

56 but also the expression of cytosolic chaperones and the ubiquitin-proteasome system, which  
57 mitigate the deleterious effects of mistargeted precursors<sup>27-29</sup>. In addition, the synthesis of many  
58 mitochondrial proteins is muted by transcriptional repression as well as global translation  
59 attenuation to further reduce the burden on cytosolic proteostasis<sup>28,30,31</sup>.

60 While numerous pathways of cross-compartment communication under proteotoxic stress have  
61 been identified, our understanding of the connections between organellar stress response programs  
62 is still incomplete. Here we show that defective mitochondrial protein import not only activates  
63 mitochondrial and cytosolic stress responses, but also triggers the unfolded protein response of the  
64 ER. This is at least in part attributable to the targeting of mitochondrial membrane proteins to the  
65 ER. The UPR<sup>ER</sup> is functionally relevant both under conditions of compromised protein import, and  
66 conditions that induce mitochondrial biogenesis such as metabolic adaptations. Thus, the UPR<sup>ER</sup>  
67 supports mitochondrial biogenesis by buffering the adverse consequences of elevated levels of non-  
68 imported mitochondrial precursor proteins.

69

70

## 71 **Results**

### 72 **The unfolded protein response of the ER is triggered by long-lasting mitoprotein-induced** 73 **stress**

74 Cellular adaptations to imbalances in mitochondrial proteostasis have been studied using mutants of  
75 protein import components<sup>27</sup>, chaperones<sup>29</sup>, folding-incompetent mitochondrial proteins<sup>31,32</sup>, or  
76 defects in the respiratory chain<sup>33,34</sup>. Many of these perturbations converge on the impairment of  
77 mitochondrial protein import. Model systems in which protein import can be acutely blocked have  
78 proven particularly useful to decipher the mechanistic details of responses to such mitoprotein-  
79 induced stress. A way of achieving this is the overexpression of mitochondrial precursor proteins  
80 that are intrinsically prone to premature folding and stalling inside the narrow mitochondrial  
81 translocases<sup>35</sup>. For instance, the well-characterized ‘clogger’ protein *b*<sub>2</sub>-DHFR can be used for this  
82 purpose<sup>28,36</sup>. This fusion protein consists of the N-terminal 167 amino acids of cytochrome *b*<sub>2</sub>  
83 (including its mitochondrial targeting signal) and the rapidly and tightly folding dihydrofolate  
84 reductase DHFR (Fig. 1A)<sup>37-39</sup>. Expression of the clogger results in accumulation of non-imported  
85 precursor proteins (Fig. 1B) and impairs cell growth (Fig. 1C). In baker’s yeast, the expression of  
86 *b*<sub>2</sub>-DHFR can be tightly controlled by using a *GAL* promoter that can be switched on by the addition  
87 of galactose to the lactate-based growth media. This allows for a tight temporal resolution and the  
88 discrimination between short-term and long-term responses to an acute and specific blockade of  
89 protein import.

90 We previously characterized the immediate reactions of the cellular transcriptome to mitoprotein-  
91 induced stress<sup>28</sup>. An induction of many chaperones and the proteasome and a repression of  
92 OXPHOS components and ribosomes all took place within 1.5 h of clogger expression, some of  
93 them even markedly earlier (Fig. 1D). However, many cellular adaptations change when acute  
94 stress persists and becomes long-lasting<sup>40-42</sup>. We therefore asked whether cells undergo additional  
95 adaptations when exposed to long-term mitoprotein-induced stress. To this end, we reanalyzed our  
96 previously collected data to examine changes in the cellular proteome after up to 18 h of clogger

97 expression<sup>28</sup>. We queried for changes in the proteome that were evident at time points no earlier  
98 than 4.5 h, which corresponds to approximately one cell doubling in respiratory medium.  
99 Interestingly, this criterion identified a group of proteins that are associated with the unfolded  
100 protein response of the ER (Fig. 1E and S1A)<sup>21</sup>. Some individual targets of the UPR<sup>ER</sup>, such as e.g.  
101 Ero1 and Kar2, were induced at earlier time points, presumably due to their responsiveness to the  
102 transcription factors Hsf1 and/or Rpn4 that form the first line of defense against mitoprotein-  
103 induced stress. Moreover, a small number of UPR targets were decreased over time. These proteins  
104 (Hem15, Mdl1, Coq6, Mgr1) almost exclusively localize to mitochondria and their levels are likely  
105 affected by the import block or the clogger-induced downregulation of mitochondrial components.  
106 However, most UPR targets showed a consistent upregulation that was observed 9 h after clogger  
107 induction, and even more so after 18 h (Fig. 1E and S1A).

108 In yeast, the UPR<sup>ER</sup> is activated by splicing of an intron from the *HAC1* mRNA in the cytosol  
109 through the ER-resident kinase Ire1. Only the spliced isoform of the mRNA (called *HAC1<sup>i</sup>*) can be  
110 translated and gives rise to a transcription factor<sup>10</sup>. To test whether *HAC1* was indeed spliced and  
111 translated under mitoprotein-induced stress, we analyzed clogger-expressing cells by ribosome  
112 profiling. Here, ribosome footprints from cells expressing *b<sub>2</sub>*-DHFR or cytosolic DHFR were  
113 sequenced 4.5 h after induction, and the changes in the translome were compared to the changes  
114 in the transcriptome (Fig. 1F). For the large majority of all genes, transcriptional and translational  
115 changes correlated tightly. For *HAC1* however, we observed a slight reduction of mRNA levels,  
116 while we found four times more ribosome footprints on *HAC1* mRNA in clogger-expressing than in  
117 control cells (Fig 1G). In fact, *HAC1* was one of the most prominent outliers in this comparison,  
118 ranking as the gene with the second-highest gain in translational efficiency when mitochondrial  
119 import was blocked (Fig. S1B). The increase in ribosome occupancy was restricted to the exon  
120 region of the mRNA, while the intron region of *HAC1* was free of ribosome densities in both  
121 conditions (Fig 1H).

122 We next sought to more precisely determine the timing of the UPR<sup>ER</sup> activation. To this end, we set  
123 up an RT-qPCR assay which quantifies the spliced isoform of *HAC1*<sup>i</sup> by using a primer-probe  
124 combination which specifically recognizes the exon-exon junction of *HAC1*<sup>i</sup> (Fig. S1C, D). We  
125 induced *b<sub>2</sub>*-DHFR by addition of 0.5% galactose to cultures that were previously grown in lactate  
126 medium and followed *HAC1* splicing over time. The earliest time point at which we could detect a  
127 considerable difference between clogger-expressing and control cells was 3 h (Fig. 1I). As a certain  
128 delay between the onset of *HAC1* splicing and downstream changes in protein levels of UPR<sup>ER</sup>  
129 targets is expected, this is consistent with our earlier observation that UPR<sup>ER</sup> induction is a rather  
130 late event in mitoprotein-induced stress signaling.

131 We conclude that under long-term impairment of mitochondrial protein import, cells induce the  
132 UPR<sup>ER</sup> via the canonical Ire1-Hac1 pathway.

133

### 134 **UPR<sup>ER</sup> induction is required for cellular fitness under mitoprotein-induced stress**

135 We asked whether UPR<sup>ER</sup> induction is functionally relevant under sustained mitoprotein-induced  
136 stress, given that its magnitude is rather mild when compared to harsh ER insults such as treatment  
137 with tunicamycin (*cf.* Fig. S1C). To this end, we compared the fitness of UPR<sup>ER</sup>-deficient cells with  
138 that of wild type cells when mitochondrial import was blocked. Indeed, when either *HAC1* or *IRE1*  
139 were deleted, cells exhibited synthetic growth defects upon clogger expression, both in liquid  
140 medium and on plates (Fig. 2A, B).

141 We examined the relevance of UPR<sup>ER</sup> signaling when mitochondrial import is impaired by an  
142 approach orthogonal to clogging the translocases. To this end, we deleted *HAC1* or *IRE1* in a strain  
143 that carries a temperature-sensitive mutation in the essential import component Mia40. Mia40 is  
144 responsible for the import and oxidative folding of cysteine-containing mitochondrial  
145 intermembrane space proteins<sup>43,44</sup>. The import defects in the *mia40-4* mutant were shown to trigger  
146 cytosolic adaptations (unfolded protein response activated by mistargeting of proteins, UPR<sup>am</sup>)

147 similar to those elicited by the clogger<sup>27</sup>. Indeed, *mia40-4* cells grew worse at semi-permissive  
148 growth conditions when *IRE1* or *HAC1* were deleted, demonstrating that UPR<sup>ER</sup> signaling is  
149 relevant when protein import into the IMS is perturbed (Fig. 2C).

150 In conclusion, defects in mitochondrial protein import trigger the UPR<sup>ER</sup>, which is required for  
151 cellular fitness under such conditions (Fig. 2D).

152

### 153 **Mitochondrial membrane proteins accumulate at the ER when mitochondrial protein import** 154 **is impaired**

155 What could be the cause for UPR<sup>ER</sup> activation in situations when mitochondrial import is impaired?  
156 Blocking import should elevate levels of mitochondrial precursor proteins in the cytosol. Therefore,  
157 we reasoned that a portion of these non-imported precursors, perhaps comprising membrane  
158 proteins, may be targeted to the ER, where they would accumulate and engage folding and protein  
159 quality control systems, thus triggering UPR<sup>ER</sup> activation.

160 To test this hypothesis, we labelled the mitochondrial inner membrane protein Oxa1 with  
161 ymNeonGreen, and coexpressed it with Sec63-ymScarletI as an ER marker, followed by analysis of  
162 their subcellular distribution by fluorescence microscopy. When we expressed cytosolic DHFR, the  
163 green Oxa1 signal and the red Sec63 signal partitioned into separate structures with no considerable  
164 colocalization. In contrast, when *b<sub>2</sub>*-DHFR was expressed for 4.5 h, we found that a fraction of  
165 Oxa1-ymNeonGreen colocalized with Sec63-ymScarletI in the typical ring-shaped structures of the  
166 perinuclear and peripheral ER (Fig. 3A). This ER co-localization was observed in around 30% of  
167 the clogger-expressing cells, but only in around 1% of control cells (Fig. 3B).

168 Fusions with fluorescent proteins can interfere with the function, localization, folding and stability  
169 of proteins<sup>45-47</sup>. In particular, a large, stably folding C-terminal moiety might generate a  
170 mitochondrial clogger, as exemplified by *b<sub>2</sub>*-DHFR itself, and interfere with import and  
171 localization. We therefore sought to verify our results by a method that avoids the fusion of large



172 protein domains to mitochondrial precursors and also minimizes the need for manual categorization  
173 of microscopic images with high mitochondrial background signal. To this end, we adapted a split-  
174 GFP method specifically designed to assess protein localization *in vivo*<sup>48</sup>. Superfolder GFP is split  
175 into two parts, GFP<sup>1-10</sup> and GFP<sup>11</sup>, which only emit fluorescence when co-localized to the same  
176 compartment (Fig. 3C). The GFP fragments do not alter the folding behavior of the fusion proteins  
177 and their affinity is high enough to promote self-association without the need for a direct protein-  
178 protein interaction of the fusion partners<sup>49-51</sup>. The GFP<sup>11</sup> tag consists of only 17 amino acid  
179 residues and is therefore unlikely to affect translocation across the mitochondrial membranes.

180 To first verify that the split-GFP assay captures the subcellular localization of mitochondrial  
181 proteins, we fused the GFP<sup>11</sup> fragment to the C-terminus of Oxa1 (inner membrane, C-terminus at  
182 matrix side), Mia40, Dld1 (inner membrane, C-terminus at IMS side) and Om45 (outer membrane,  
183 C-terminus at IMS side) and the GFP<sup>1-10</sup> fragment to Oxa1 (IM, matrix side), Mia40 (IM, IMS  
184 side), Sec63 (ER membrane, cytosolic side) and Ssa1 (cytosol) (Fig. S2A)<sup>52-58</sup>. In the absence of  
185 any stress, the by far strongest fluorescence signal was detected for the combinations that  
186 recapitulate the known localization and topology for all proteins tested (Oxa1-GFP<sup>11</sup> / Oxa1-GFP<sup>1-</sup>  
187 <sup>10</sup>, Mia40-GFP<sup>11</sup> / Mia40-GFP<sup>1-10</sup>, Dld1-GFP<sup>11</sup> / Mia40-GFP<sup>1-10</sup>, Om45-GFP<sup>11</sup> / Mia40-GFP<sup>1-10</sup>),  
188 while all other combinations resulted in much lower fluorescent signals (Fig. 3D and S2B-D,  
189 control condition in blue). This showed that the approach can measure protein localization with sub-  
190 organellar resolution.

191 We next expressed either *b*<sub>2</sub>-DHFR or cytosolic DHFR for 4.5 h in strains carrying the split-GFP  
192 reporters. *b*<sub>2</sub>-DHFR expression evoked a marked increase in signal for Oxa1-GFP<sup>11</sup> with the Sec63-  
193 GFP<sup>1-10</sup> and the Ssa1-GFP<sup>1-10</sup> reporters, while with cytosolic DHFR, only very little signal was  
194 detected (Fig. 3D). This points towards relocation of a fraction of newly synthesized Oxa1-GFP<sup>11</sup> to  
195 the ER surface or, potentially, the cytosol. We used fluorescence microscopy to confirm that the  
196 fluorescence we measured in a plate reader setup indeed originated from ER-localized GFP  
197 complementation (Fig. 3E and S2E-F). For the mitochondrial outer membrane protein Om45-

198 GFP<sup>11</sup>, we found a similar redistribution to the ER under import stress (Fig. 3F and S2B), while  
199 neither Mia40-GFP<sup>11</sup> nor Dld1-GFP<sup>11</sup> showed detectable ER localization (Fig. S2C, D). Obviously,  
200 some but not all mitochondrial membrane proteins are routed to the ER when their entry into  
201 mitochondria is delayed.

202 How is the timing of precursor localization to the ER after mitochondrial import is blocked? To  
203 assess this question, we grew cells expressing Oxa1-GFP<sup>11</sup> and Sec63-GFP<sup>1-10</sup> in a plate reader,  
204 induced *b<sub>2</sub>*-DHFR or cytosolic DHFR by addition of galactose and monitored split-GFP  
205 fluorescence over time in living cells. Constitutively expressed ymScarletI was used to normalize  
206 for differences in cell growth and translation rates. Clogger-expressing cells showed elevated split-  
207 GFP signals from around 3 h after induction (Fig. 3G). Strikingly, the induction of the UPR<sup>ER</sup> and  
208 the detection of Oxa1 at the ER perfectly coincided in time (*cf.* Fig. 1I).

209 In conclusion, when mitochondrial import is blocked, some mitochondrial preproteins accumulate  
210 at the ER membrane which likely evokes the UPR<sup>ER</sup> (Fig. 3H).

211

## 212 **The UPR<sup>ER</sup> maintains cellular fitness during adaptation of mitochondrial biogenesis**

213 Is the UPR<sup>ER</sup> only a stress-reactive system that comes into play when mitochondrial import is  
214 defective, or is it of more general relevance for mitochondrial biogenesis? Accurate protein sorting  
215 is a challenging task for cells, and the ER might constantly encounter a certain load of  
216 mitochondrial precursor proteins. To check whether there is evidence for mitochondrial proteins  
217 routed to the ER in the absence of stress, we reanalyzed several high-resolution datasets on protein  
218 targeting. Proximity labeling of ribosomes close to the ER or the mitochondrial outer membrane  
219 and subsequent ribosome profiling determined the ‘local translome’ at the ER and mitochondrial  
220 surface in yeast<sup>59,60</sup>. Interestingly, while most mitochondrial proteins were enriched in the vicinity  
221 of mitochondria, a subset of mitochondrial proteins was found to be translated close to the ER,  
222 notably including Oxa1 (Fig. 4A). Also in human cells, mRNAs of some mitochondrial proteins

223 were found at the ER surface (Fig. S3A)<sup>61</sup>. Finally, we reanalyzed datasets from studies that  
224 determined which nascent chains interact with the signal recognition particle (SRP) in yeast by  
225 pulldown of SRP and subsequent sequencing of the bound transcripts<sup>62,63</sup>. SRP is a major targeting  
226 factor for secretory proteins that carry a signal sequence or transmembrane domains<sup>64-67</sup>. While  
227 secretory proteins were clearly the most enriched among the SRP substrates, a subset of  
228 mitochondrial encoding ribosome-nascent chains were also bound by SRP to a lesser extent, but  
229 significantly above what was found for cytosolic proteins (Fig. S3B). Both in yeast and in human  
230 cells, ER-localized mitochondrial transcripts include, but are not limited to proteins with known  
231 dual localization to mitochondria and ER. Apparently, some mitochondrial precursors have a  
232 tendency to be targeted to the ER even in the absence of stress, possibly mediated by ‘low priority’  
233 SRP-binding to at least some of these precursors.

234 We did not observe considerable fluorescence in our split-GFP assays without applying import  
235 stress. However, under steady state conditions, precursors might only very transiently localize to the  
236 ER because they can be efficiently rerouted to mitochondria with the help of the ER-resident J  
237 protein Djp1 in a process called ER-SURF<sup>15</sup>. Loss of this pathway does not impair mitochondrial  
238 import *per se*, but would trap mitochondrial orphans at the ER. To test this, we employed our split-  
239 GFP assay in the ‘ER-trapping’ *Δdjp1* mutant and found accumulation of Oxa1 at the ER even  
240 under optimal growth conditions (Fig. 4B). Hence, there is indeed a constitutive flux of  
241 mitochondrial precursors to the ER in the absence of stress.

242 We therefore wondered whether the UPR<sup>ER</sup> might be required to buffer fluctuations in the levels of  
243 ER-localized mitochondrial precursors under physiological conditions. Mitochondrial biogenesis is  
244 strongly dependent on the carbon source in the growth media: The levels and, hence, synthesis of  
245 many mitochondrial proteins are low on glucose, but considerably higher on raffinose, galactose,  
246 glycerol or lactate<sup>68-70</sup>. In fact, we observed that the extent of steady state *HAC1* splicing was low  
247 when cells were grown on glucose, but elevated on all other carbon sources, particularly on  
248 galactose and glycerol (Fig. 4C). To assess the functional relevance of the UPR<sup>ER</sup> under different

249 states of mitochondrial metabolism, we grew wild type,  $\Delta hac1$  and  $\Delta ire1$  cells to exponential phase  
250 in liquid medium containing glucose, galactose or lactate as sole carbon source. Then we washed  
251 the cells, resuspended them in glucose, galactose and lactate medium in all possible combinations  
252 and monitored their growth (Fig. 4D). While there was no difference between wild type and ER-  
253 deficient strains when they remained in the media they were cultured in before,  $\Delta hac1$  and  $\Delta ire1$   
254 mutants had problems to adapt when carbon sources were switched to a medium with higher levels  
255 of *HAC1* splicing. Likewise, ER-deficient strains grew well during exponential phase in glucose,  
256 but exhibited a phenotype at high optical densities, shortly before the cultures entered the stationary  
257 phase. At this point, yeast cells respond to the depletion of glucose and switch to respiratory  
258 metabolism, a growth phase called diauxic shift in which mitochondrial biogenesis is strongly  
259 induced<sup>71,72</sup>. Hence, the UPR<sup>ER</sup> is important when such a remodeling takes place.

260 Would a stronger UPR<sup>ER</sup> help cells to adapt to respiratory growth conditions? Yeast cells grew  
261 better on respiratory media when exposed to moderate amounts of the reducing agent dithiothreitol  
262 (DTT), which is a known trigger of the UPR<sup>ER</sup> and, consequently, is toxic for UPR-deficient strains  
263 (Fig. 4E). However, its beneficial effect on respiratory growth might – at least in part – also result  
264 from UPR<sup>ER</sup>-independent effects. We therefore sought to induce the UPR<sup>ER</sup> directly without any  
265 stress treatment by expressing the spliced isoform of *HAC1* from a  $\beta$ -estradiol-inducible *GAL*  
266 promoter<sup>23</sup>. Cells were precultured in glucose medium and, upon shift to either glucose or lactate  
267 medium, exposed to various  $\beta$ -estradiol concentrations, i.e. to different levels of *HAC1<sup>i</sup>* expression.  
268 Indeed, cells grew better in lactate when *GAL-HAC1<sup>i</sup>* was induced with up to 50 nM  $\beta$ -estradiol,  
269 while they were not affected when grown in glucose (Fig. 4F). Higher concentrations of  $\beta$ -estradiol  
270 delayed growth, consistent with earlier reports that overshooting UPR<sup>ER</sup> activation can be toxic<sup>73,74</sup>.

271 Obviously, a functional UPR<sup>ER</sup> is not only important when mitochondrial protein import is blocked,  
272 but also maintains cellular fitness under physiological conditions with elevated mitochondrial  
273 biogenesis. We propose that a fraction of mitochondrial precursor proteins is always localizing to  
274 the ER, either transiently as part of the ER-SURF pathway or terminally mistargeted. When the

275 influx of precursors is altered due to changes in gene expression or by mitochondrial dysfunction,  
276 the UPR<sup>ER</sup> acts as a ‘rheostat’ and adjusts the protein folding and quality control components of the  
277 ER accordingly (Fig. 4G).

278

## 279 **Discussion**

280 Precursor proteins that accumulate outside mitochondria impose a burden on cellular proteostasis.  
281 Many precursors remain in the cytosol<sup>31</sup> or end up in the nucleus<sup>75</sup>, where chaperones and the  
282 proteasome mitigate the adverse effects of mistargeted proteins and eventually degrade them  
283<sup>27,28,76,77</sup>. Membrane proteins are particularly prone to misfolding and aggregation in an aqueous  
284 environment. Hence, their prolonged presence in the cytosol can be very hazardous for cells<sup>78,79</sup>.  
285 We found in this study that cells can adsorb precursors of mitochondrial membrane proteins to the  
286 surface of the ER and employ the UPR<sup>ER</sup> to buffer their elevated levels at the ER. Apparently,  
287 mitochondrial proteins associate with the ER even under physiological conditions. However, the  
288 accumulation of mitochondrial precursors at the ER is exacerbated by import defects as well as by  
289 metabolic stimuli that increase the expression of abundant mitochondrial enzymes, many of which  
290 are membrane proteins. Our observations identify the UPR<sup>ER</sup> as an important cellular response to  
291 promote cellular fitness under such conditions, especially during the phase of adaptation.

292 There are numerous reasons why engaging the ER as a venue for buffering mitochondrial  
293 membrane proteins can be beneficial: (1) The large ER membrane provides a favorable  
294 environment for proteins with hydrophobic transmembrane domains that would otherwise misfold  
295 in the aqueous cytosol. (2) The ER has a remarkable capacity to prevent protein aggregation, even  
296 exceeding that of the cytosol for some classes of proteins<sup>80,81</sup>. (3) Besides having chaperones that  
297 promote protein folding, the ER harbors an elaborate machinery for ER-associated protein  
298 degradation (ERAD). ER components have been found to participate in the degradation of cytosolic  
299 and, more recently, mitochondrial proteins<sup>82,83</sup>. (4) ER and mitochondria share many components  
300 in their protein biogenesis and quality control systems, e.g. the Hsp40 co-chaperone Ydj1 or  
301 Cdc48/VCP/p97 and many of its cofactors<sup>36,84-86</sup>. In addition, some organelle-specific factors of ER  
302 and mitochondria physically interact and functionally cooperate with each other<sup>87</sup>. (5) Protein  
303 transfer between mitochondrial and ER membranes is possible via dedicated machineries that can  
304 extract mislocalized proteins from the membrane and set them back en route to the respective other

305 organelle<sup>15,88-91</sup>. (6) The close proximity of mitochondria and ER at membrane contact sites might  
306 facilitate the exchange of proteins between the two organelles. Interestingly, ER-mitochondria  
307 contact sites are enriched with ER chaperones and other UPR<sup>ER</sup> effectors<sup>92</sup> and their loss activates  
308 the UPR<sup>ER</sup><sup>93</sup>. In addition, contact sites are crucial for the initiation of autophagy<sup>94,95</sup>.

309 Based on the above considerations, it is possible that routing of mitochondrial precursors to the ER  
310 could be more than a mere ‘mistake’ in protein targeting, but rather an actively regulated quality  
311 control pathway. In line with this idea, our analyses show that SRP recognizes and binds nascent  
312 chains of some mitochondrial proteins, suggesting that a portion of the mitochondrial proteome is  
313 synthesized at the ER surface. Also the GET pathway (guided entry of tail-anchored proteins) was  
314 recently identified to be involved in ER targeting of mitochondrial tail-anchored proteins and some  
315 carrier proteins<sup>88,96</sup>.

316 Our findings add to a significant body of observations linking the stress responses and homeostasis  
317 mechanisms of mitochondria and ER<sup>97</sup>. Several processes connect mitochondrial and ER  
318 homeostasis in the context of stress: the flux of lipids between mitochondrial and ER membranes<sup>98</sup>;  
319 the generation of ATP as well as reactive oxygen species by the respiratory chain<sup>99,100</sup>; the transport  
320 of calcium<sup>16,101</sup>; or the availability of building blocks for glycosylation of secretory proteins,  
321 provided by mitochondrial carbohydrate metabolism<sup>102</sup>. We propose that mitochondria and ER are  
322 also linked in the management of mitochondrial biogenesis.

323 Our findings open the question which of the many components and pathways that are reinforced by  
324 the UPR<sup>ER</sup> are the most important for the management of ER-localized mitochondrial proteins. It  
325 will be exciting to disentangle the exact contributions of storage and handling of misfolding-prone  
326 precursors, their transfer to mitochondria or their degradation at the ER surface.

327 We suggest that cells engage the ER and its proteostasis capacity – augmented by the UPR<sup>ER</sup> when  
328 necessary – as a buffer for proteins that can’t be immediately imported into mitochondria. From  
329 there, they can be either degraded or kept on hold for a second attempt of mitochondrial import.

330 Therefore, we should consider to rethink the classical concept of ‘mislocalization’ as a problem that  
331 cells need to avoid. Rather, spatial sequestration (transient or terminal) of proteins to compartments  
332 other than those they are primarily targeted to might be a productive step in protein biogenesis. It  
333 will be exciting to explore this concept and the components that are involved in the future.

334

335

336



## 337 **Materials and Methods**

### 338 **Yeast strains and plasmids**

339 All yeast strains used in this study are listed in Supplementary Table S1 and were based on the wild  
340 type strain W303 or YPH499<sup>103,104</sup>. The *mia40-4* strain was a gift from Agnieszka Chacinska<sup>44</sup>.

341 Yeast strains were grown on YP medium (1% yeast extract, 2% peptone) or synthetic medium  
342 (0.17% yeast nitrogen base and 0.5% (NH<sub>4</sub>)<sub>2</sub>SO<sub>4</sub>) containing 2% glucose, 2% galactose, 2%  
343 raffinose, 2% glycerol or 2% lactate and supplemented with appropriate amounts of amino acids  
344 and nucleobases for selection.

345 pFA6a-ymNeongreen-*CaURA3* and pFA6a-ymScarletI-*CaURA3* were kindly provided by Bas  
346 Teusink (Addgene plasmids # 125703 and # 118457)<sup>105</sup>. Genomic tagging with ymNeonGreen was  
347 performed by amplifying the ym-NeonGreen-*CaURA3* cassette with overhangs homologous to the  
348 *OXA1* locus and transforming yeast cells using the lithium acetate/ss carrier DNA/PEG method<sup>106</sup>.

349 Genomic deletion of *IRE1* and *HAC1* in the *mia40-4* background was performed by amplifying a  
350 kanMX4 cassette from a pFA6a plasmid with overhangs homologous to the sequences up- and  
351 downstream of the genomic open reading frames of the target genes<sup>106</sup>. Yeast cells were  
352 transformed with the PCR product and grown on plates containing 150 µg/ml G418 for selection.  
353 Deletions were confirmed by colony PCR on the targeted genomic loci.

354 The sequences of GFP<sup>11</sup> (pSJ1321, pRS315-NOP1pr-GFP11-mCherry-PUS1) and GFP<sup>1-10</sup>  
355 (pSJ2039, pRS316-NOP1pr-GFP1-10-SCS2TM) were a gift from Sue Jaspersen (Addgene  
356 plasmids # 86413 and # 86418)<sup>48</sup>. Cloning of the split-GFP constructs into the pYX122, pYX142  
357 and pNH605 plasmids used in this study was performed by Gibson Assembly with the HiFi DNA  
358 Assembly Master Mix (New England Biolabs, #E2621L) according to the manufacturer's  
359 instructions. The GFP<sup>11</sup> part was fused to the different proteins by integration of the sequence  
360 (5' AGA GAT CAT ATG GTT TTG CAT GAA TAT GTT AAT GCT GCT GGT ATT ACT  
361 TAA 3') into the corresponding primers. GFP<sup>1-10</sup> was amplified from the plasmid (pSJ2039) with  
362 overhangs homologous to the end of the fusion partner and the plasmid pYX122.

### 363 **Isolation of RNA and RT-qPCR**

364 RNA was extracted from yeast cells using either the acid phenol-chloroform method or an RNeasy  
365 Mini kit with on-column removal of DNA (Qiagen), both as previously described<sup>28</sup>. In either case,  
366 3 OD<sub>600</sub>×ml of cells were collected by centrifugation (17,000 × g, 3 min, 2°C), washed with  
367 prechilled water, snap-frozen in liquid nitrogen and stored at -80°C.

368 For acid phenol-chloroform extraction, cell lysates were prepared in lysis buffer (50 mM Tris/HCl  
369 (pH 7.0), 130 mM NaCl, 5 mM EDTA, 5% (w/v) SDS) with a FastPrep-24 5 G homogenizer (MP  
370 Biomedicals) with 3 cycles of 20 s, speed 6.0 m s<sup>-1</sup>, 120 s breaks, lysis matrix Y). RNA was  
371 purified with repeated extraction with acid phenol–chloroform (5:1, pH 4.5, two times) and 24:1  
372 chloroform–isoamylalcohol (24:1). Then, 0.3 M sodium acetate (pH 5.5) was added, RNA was  
373 precipitated with ethanol and solubilized in water. DNA was removed using a Turbo DNA Free kit  
374 (Ambion) following the manufacturer’s instructions. RNA purity and concentration were assessed  
375 using a DeNovix DS-11 FX+ Fluorometer.

376 RT-qPCR was performed with a CFX96 Touch Real-Time PCR Detection System (Bio-Rad). 100  
377 ng total RNA per 20 µl reaction were analyzed using the Luna Universal Probe One-Step RT-qPCR  
378 Kit (NEB, # E3006) in technical triplicates. cDNA was generated by reverse transcription for 10  
379 min at 55°C. PCR amplification was then carried out under the following conditions: initial  
380 denaturation for 1 min at 95°C, followed by 45 cycles of 10 s at 95°C (denaturation) and 30 s at  
381 60°C (extension). Primer-probe combinations for qPCR are listed in Supplementary Table 3. For  
382 the specific detection of the spliced isoform of *HAC1*, primers were chosen to flank the intron and  
383 the fluorescent probe spans the exon-exon junction (Fig. S1B). Primer efficiency was determined by  
384 measuring serial dilutions of pooled cDNA and only primer-probe combinations with an efficiency  
385 within 90% and 110% were used.  $C_q$  values were obtained with the Bio-Rad CFX Manager 3.1 with  
386  $C_q$  Determination Mode set to “Single Threshold” and Baseline Setting set to “Baseline Subtracted  
387 Curve Fit”. Gene expression was normalized to the geometric mean of the expression values of the

388 reference gene *TFCI*<sup>107</sup>. Statistical significance was assessed with paired two-tailed Student's *t*-  
389 test.

### 390 **Growth Assays**

391 Growth curves were performed automated in a 96 well plate in technical triplicates using the  
392 ELx808 Absorbance Microplate Reader (BioTek). Precultures of 100  $\mu$ l were inoculated at an  
393 OD<sub>600</sub> of 0.1 in round bottom microtiter plates and sealed with an air-permeable membrane  
394 (Breathe-Easy; Sigma-Aldrich, St. Louis, MO). The growth curves started at OD<sub>600</sub> 0.1 and  
395 incubated at 30°C for 72 h under constant shaking. The OD<sub>600</sub> was measured every 10 min.

396 For the Halo assay, strains were grown in liquid YPD media to mid-log phase, washed and plated  
397 on YPG plates. A filter plate was placed onto the plate and soaked with 10  $\mu$ l of a 3 M DTT  
398 solution. Plates were incubated at 30°C for 2 days.

399

### 400 **Preparation of Cell Extracts for Western Blotting**

401 For whole cell lysates yeast strains were cultivated in selective lactate media. Clogger expression  
402 was induced by adding 0.5% galactose. After 4.5h, 2 OD<sub>600</sub>×ml of cells were harvested by  
403 centrifugation (5,000g, 5 min, RT) and washed with water. The cells were resuspended in 40  
404  $\mu$ l/OD<sub>600</sub> 1x Laemmli buffer (125 mM Tris/HCl (pH 6.8), 5% SDS (w/v), 25% glycerol, 0.0005%  
405 bromophenol blue) and transferred to a screw-cap tube containing glass beads (0.5 mm). Cell were  
406 lysed using a FastPrep-24 5 G homogenizer (MP Biomedicals) with 3 cycles of 20 s, speed 6.0 m/s,  
407 120 s breaks, lysis matrix Y. Cell extracts were boiled for 10 min at 96°C. Samples were stored at -  
408 20°C until usage. An equal amount of lysate corresponding to 0.4 OD<sub>600</sub>×ml per sample was loaded  
409 on an SDS gel.

410

### 411 **Immunoblotting**

412 Proteins were separated by size using discontinuous sodium dodecyl sulfate polyacrylamide gel  
413 electrophoresis (SDS-PAGE). They were transferred to a nitrocellulose membrane by semi-dry  
414 western blotting with blotting buffer (20 mM Tris, 150 mM glycine, 0.08% SDS (w/v), 20%  
415 methanol). To visualize the transferred proteins, the membrane was stained with Ponceau S solution  
416 (0.2% (w/v) Ponceau S, 3% (w/v) acetic acid) for 5 min. The membrane was cut in pieces to  
417 decorate against several antibodies at once and unspecific binding was blocked by incubation for 30  
418 min in 5% milk in 1X TBS buffer (10 mM Tris/HCl (pH 7.5), 150 mM NaCl). The first antibodies  
419 were incubated over night at 4°C. The membrane was washed extensively with 1X TBS Buffer.  
420 Afterwards, the membrane was incubated for 90 min at room temperature with the secondary  
421 antibody containing the horseradish peroxidase (anti-Rabbit). The membrane was again washed  
422 extensively before ECL1 (100 mM Tris/HCl (pH 8.5), 0.044% (w/v) luminol, 0.0066% p-coumaric  
423 acid) and ECL2 (100 mM Tris/HCl (pH 8.5), 0.03% H<sub>2</sub>O<sub>2</sub>) solutions were mixed 1:1 and poured  
424 onto the membrane. Thereby chemo luminescence is produced by horseradish peroxidase coupled  
425 to the secondary antibody, which was detected on Super RX Medical X-Ray Films (Fuji) using the  
426 Optimax Type TR-developer.

427

#### 428 **Antibodies**

429 The antibodies for the use in immunoblotting of *S. cerevisiae* cell extracts were raised in rabbits  
430 using purified recombinant proteins. The secondary antibody was ordered from Biorad (Goat anti-  
431 Rabbit IgG (H+L)-HRP Conjugate #172-1019). Antibodies were diluted in 5% (w/v) nonfat dry  
432 milk-TBS (Roth T145.2) with the following dilutions: anti-Sod1 1:1,000, anti-Rip1 1:750, anti-  
433 Mdj1 1:125, anti-Rabbit 1:10,000. anti-Rip1 and anti-Mdj1 sera were a gift from Thomas Becker.

434

#### 435 **Split-GFP Assay**

436 Cells containing were transformed with one of the plasmids pYX142-Oxa1-GFP<sup>11</sup>, pYX142-Om45-  
437 GFP<sup>11</sup>, pYX142-Dld1-GFP<sup>11</sup> or pYX142-Mia40-GFP<sup>11</sup> in combination with either pYX122-Sec63-  
438 GFP<sup>1-10</sup>, pYX122-Oxa1-GFP<sup>1-10</sup>, pYX122-Mia40-GFP<sup>1-10</sup> or pYX122-Ssa1-GFP<sup>1-10</sup>. All  
439 combinations contained also either the plasmid pYX233-*b*<sub>2</sub>-DHFR or the control plasmid pYX233-  
440 *cyt* DHFR. Cells were grown in selective medium containing 2% lactate to mid log phase.  
441 Mitoprotein-induced stress was induced by addition of 0.5% galactose for 4.5 h. 3 OD<sub>600</sub>×ml were  
442 harvested, resuspended in 100 µl medium containing 2% lactate, transferred into a black 96 well  
443 plate and centrifuged (5 min at 30 g). The fluorescence was measured with the excitation/emission  
444 wavelengths 485±15/530±20 nm in a fluorescence microplate reader (Clariostar, BMG labtech).

445 For the time course measurement of split-GFP fluorescence in a growing culture, the split-GFP  
446 cassette with Oxa1-GFP<sup>11</sup> and Sec63-GFP<sup>1-10</sup> was genomically integrated into the *LEU2* locus of  
447 yeast cells. In addition, a constitutively expressed *TEF1p*-ymScarletI was integrated into the *HIS3*  
448 locus. The cells were transformed with a pYX233 plasmid for either cytosolic DHFR or *b*<sub>2</sub>-DHFR  
449 expression and grown to mid-log phase in synthetic lactate medium. The cells were then diluted to  
450 an OD<sub>600</sub> of 0.4 in 100 µl lactate medium with (inducing) or without (non-inducing) 0.5% galactose  
451 in a microtiter plate sealed with an air-permeable membrane (Breathe-Easy; Sigma-Aldrich, St.  
452 Louis, MO) in *n*=6 replicates. A WT strain not expressing no fluorescent protein was used for  
453 correction of the background fluorescence of cells or media. The plate was incubated at 30°C under  
454 recurrent shaking in a ClarioStar spectrofluorometer (BMG Labtech) and fluorescence was  
455 measured every 10 min with the following excitation/emission wavelengths: 485±15/530±20 nm for  
456 split-GFP and 580±15/631±36 nm for ymScarletI. Background fluorescence was subtracted and  
457 the split-GFP signal was divided by the ymScarletI signal to control for growth and overall  
458 translation. The average fluorescence intensity at timepoint 0 was set to 1.

459

460 **Fluorescence microscopy**

461 To analyze the localization of the fluorescence signal in the different split-GFP combinations, mid  
462 log phase cultures were shifted to media containing 0,5% galactose to induce the expression of the  
463 *b<sub>2</sub>*-DHFR clogger or cytosolic DHFR as control. After centrifugation of 1 OD<sub>600</sub>×ml of cells (1 min  
464 at 16.000 g at RT), the cells were resuspended in 50 µl sterile water. The cell suspension was  
465 transferred to a microscope slide for fluorescence imaging using the HCX PL APO 63x oil  
466 immersion objective of a Leica TCS SP5II confocal laser scanning microscope. GFP was excited at  
467 488 nm and emission was detected by a photomultiplier through a 530/30-nm band pass filter.  
468 Microscopy images were processed using Leica software LAS X (v3.3) and Fiji (v2.1.0).

469

## 470 **Ribosome Profiling**

### 471 *Library Preparation*

472 Yeast cultures were grown to mid-log phase in minimal medium containing 2% lactate. Expression  
473 of *b<sub>2</sub>*-DHFR or cytosolic DHFR was induced by addition of 0.5% galactose for 4.5 h. Cells were  
474 harvested by vacuum filtration (pore size 0.45 µm). In one out of three independent replicates,  
475 100 µg/ml cycloheximide was added to the yeast culture 2 min before harvesting and lysis to inhibit  
476 translation elongation, while in the other replicate, cells were not in contact with cycloheximide  
477 prior to cell lysis. Cells were flash-frozen in liquid nitrogen and lysed in a mixer mill (Retsch, MM  
478 301) in lysis buffer (20 mM Tris/HCl (pH 7.4), 140 mM KCl, 1.5 mM MgCl<sub>2</sub>, 0.5 mM DTT, 100  
479 µg/ml cycloheximide, 1% (v/v) Triton X-100) in 50 ml stainless steel grinding chambers under  
480 cryogenic conditions for 1 min at 20 Hz. Lysates were thawed in a water bath at room temperature,  
481 immediately followed by centrifugation at 15,000 g at 4°C for 10 min. RNA concentration was  
482 quantified with a NanoDrop fluorometer (absorbance at 260 nm) and RNA digestion was performed  
483 with RNase I (Ambion, #AM2294, 2.5 µl / mg RNA) for 45 min at room temperature. Digestion  
484 was stopped by the addition of SUPERase-In RNase inhibitor (Ambion, #AM2696, 2 µl / 100 µl  
485 digestion). Ribosomes were isolate by centrifugation through a 25% (w/v) sucrose cushion in a

486 TLA 100.2 rotor (Beckman) at 72,000 rpm for 20 min at 4°C. RNA was extracted from the  
487 ribosomal pellet using the hot SDS-Phenol-Chloroform method and 24-35 nt ribosome footprints  
488 were size selected on a 15% (w/v) polyacrylamide TBE-urea gel. Ribosomal RNA was removed  
489 with the RiboZero Gold kit (Illumina). Sequencing libraries were then prepared as previously  
490 described<sup>108</sup>. Libraries were quantified by qPCR (Kapa Biosystems) and sequenced using a HiSeq  
491 4000 (Illumina).

#### 492 *Data analysis*

493 Sequencing reads were demultiplexed with Illumina CASAVA v1.8 and adaptor sequences were  
494 trimmed using Cutadapt v2.8. Reads that mapped to ribosomal RNAs were removed using Bowtie  
495 v.1.2.3<sup>109</sup> and remaining reads were aligned to the yeast reference genome obtained from the  
496 *Saccharomyces* genome database (genome release R64-2-1).

497 For each read, reads were summed at each nucleotide by customized python scripts. Metagene  
498 analysis was performed separately on each fragment length to remove lengths that did not exhibit  
499 the 3-nucleotide periodicity that is characteristic for ribosome footprints. Each of the remaining  
500 reads was assigned to the first A-site nucleotide. To this end, a nucleotide offset from the 5' end of  
501 each fragment length was empirically determined, using the characteristic high ribosome density at  
502 the start codon. Nucleotide reads at each codon were then summed and used for all downstream  
503 analysis.

504 Gene-level differential expression analysis was performed using HTSeq<sup>110</sup> and the DESeq2  
505 package<sup>111</sup> within the Bioconductor v3.12 project in the statistical programming language R v.4.0.3  
506<sup>112</sup>.

507

#### 508 **Analysis of published datasets on mRNA localization**

509 The dataset on translation close to the ER and mitochondrial surface in yeast was obtained from Jan  
510 et al. (2014)<sup>59</sup>. In this study, the authors fused the biotin ligase BirA to Sec63 (ER) or Om45

511 (mitochondrial) and pulled down ribosomes that were biotinylated after a short pulse of biotin and  
512 translation inhibition with cycloheximide (CHX). The genes were filtered for those that code for  
513 mitochondrial proteins according to <sup>70</sup> and log<sub>2</sub> fold enrichments of ribosome footprints at the ER (7  
514 min CHX) or mitochondrial membranes (2 min CHX) over total ribosome footprints were plotted.

515 The dataset on transcript localization in human cells was obtained from Fazal et al. (2019)<sup>61</sup>. Here,  
516 the authors used the biotin ligase APEX2 fused to proteins of different cellular localizations to  
517 directly biotinylate RNA. Mitochondrial genes were filtered according to MitoCarta 3.0 <sup>113</sup> and log<sub>2</sub>  
518 fold enrichment of ER- or mitochondria-localized transcripts over total transcripts were plotted.

519 The dataset on the SRP-bound translome in yeast was obtained from Chartron et al. (2016)<sup>63</sup>. The  
520 authors compared ribosome-nascent chain complexes purified by pulldown of SRP to total  
521 ribosomes by ribosome profiling. Genes coding for secretory, cytosolic and mitochondrial proteins  
522 were filtered according to the author's categorization and the distribution of the log<sub>2</sub> fold  
523 enrichment of SRP-bound polysomes over total ribosome footprints was plotted.

524

## 525 **Data and material availability**

526 The data produced in this study are presented in this published article and its supplementary  
527 material. The ribosome profiling data on clogger-expressing yeast cells are deposited into GEO <sup>114</sup>  
528 with accession number GSE172017.

529 All yeast strains, plasmids and primers used in this study are listed in Supplementary Tables 1-3 and  
530 are available from the authors upon request. The plasmids pYX233 DHFR and pYX233 *b*<sub>2</sub>-DHFR  
531 for expression of the mitochondrial clogger are available via Addgene (plasmids #163761 and  
532 #163759).

533



534 **Author contributions**

535 F.B. and J.F. conceived and supervised the study. F.B. and K.C.S. prepared the ribosome profiling  
536 libraries and performed the bioinformatics analysis of the sequencing data. K.K., L.K., C.G. and  
537 F.B. generated constructs and strains. K.K., L.K. and C.G. performed *in vivo* experiments. K.K. and  
538 F.B. analyzed *HAC1* splicing by RT-PCR. K.K. established and performed the split-GFP assay.  
539 K.K. performed fluorescence microscopy and K.K. and K.G.H. analyzed the results. K.G.H. and  
540 F.B. analyzed ribosome profiling data on localized and SRP-bound translation of mitochondrial  
541 proteins. K.K., C.G., L.K., K.G.H., J.M.H., J.F. and F.B. analyzed the data. F.B. wrote the  
542 manuscript with input from all authors.

543

544 **Acknowledgements**

545 Sequencing was performed at the UCSF Center for Advanced Technology. We thank Sabine Knaus,  
546 Andrea Trinkaus and Natalia M. Barbosa for assistance with the experiments and Torsten  
547 Möhlmann for help with the microscopy. We thank T. Kelly Rainbolt and Sebastian Schuck for  
548 discussions and comments on the manuscript. This project was funded by grants from the  
549 Landesforschungsinitiative Rheinland-Pfalz BioComp (to F.B. and J.M.H.), the Deutsche  
550 Forschungsgemeinschaft (DE2803/10 to J.M.H.), the US National Institutes of Health (NIH  
551 GM56433 to J.F. and AG047126 to K.C.S.), the Glenn Foundation for Medical Research  
552 (Postdoctoral Fellowship to K.C.S.), the Company of Biologists (Travelling Fellowship  
553 JCSTF181148 to F.B.), the European Molecular Biology Organization (Long-Term Fellowship  
554 ALT 762-2019 to K.G.H.), the Helen Hay Whitney Foundation (F-1240 to K.G.H.) and the Joachim  
555 Herz Stiftung (to F.B. and C.G.).

556

557 **Competing interests**

558 The authors declare that they have no competing interests.



## 560 References

- 561 1 Klaips, C. L., Jayaraj, G. G. & Hartl, F. U. Pathways of cellular proteostasis in aging and disease. *J Cell*  
562 *Biol* **217**, 51-63, doi:10.1083/jcb.201709072 (2018).
- 563 2 Hipp, M. S., Park, S. H. & Hartl, F. U. Proteostasis impairment in protein-misfolding and -aggregation  
564 diseases. *Trends Cell Biol* **24**, 506-514, doi:10.1016/j.tcb.2014.05.003 (2014).
- 565 3 Gidalevitz, T., Ben-Zvi, A., Ho, K. H., Brignull, H. R. & Morimoto, R. I. Progressive disruption of  
566 cellular protein folding in models of polyglutamine diseases. *Science* **311**, 1471-1474,  
567 doi:10.1126/science.1124514 (2006).
- 568 4 Moehle, E. A., Shen, K. & Dillin, A. Mitochondrial proteostasis in the context of cellular and  
569 organismal health and aging. *J Biol Chem* **294**, 5396-5407, doi:10.1074/jbc.TM117.000893 (2019).
- 570 5 Aviner, R. & Frydman, J. Proteostasis in Viral Infection: Unfolding the Complex Virus-Chaperone  
571 Interplay. *Cold Spring Harb Perspect Biol* **12**, doi:10.1101/cshperspect.a034090 (2020).
- 572 6 Naresh, N. U. & Haynes, C. M. Signaling and Regulation of the Mitochondrial Unfolded Protein  
573 Response. *Cold Spring Harb Perspect Biol* **11**, a033944, doi:10.1101/cshperspect.a033944 (2019).
- 574 7 Karagöz, G. E., Acosta-Alvear, D. & Walter, P. The Unfolded Protein Response: Detecting and  
575 Responding to Fluctuations in the Protein-Folding Capacity of the Endoplasmic Reticulum. *Cold*  
576 *Spring Harb Perspect Biol* **11**, a033886, doi:10.1101/cshperspect.a033886 (2019).
- 577 8 Pincus, D. Regulation of Hsf1 and the Heat Shock Response. *Adv Exp Med Biol* **1243**, 41-50,  
578 doi:10.1007/978-3-030-40204-4\_3 (2020).
- 579 9 Münch, C. The different axes of the mammalian mitochondrial unfolded protein response. *BMC Biol*  
580 **16**, 81, doi:10.1186/s12915-018-0548-x (2018).
- 581 10 Cox, J. S. & Walter, P. A novel mechanism for regulating activity of a transcription factor that  
582 controls the unfolded protein response. *Cell* **87**, 391-404, doi:10.1016/s0092-8674(00)81360-4  
583 (1996).
- 584 11 Walter, P. & Ron, D. The unfolded protein response: from stress pathway to homeostatic  
585 regulation. *Science* **334**, 1081-1086, doi:10.1126/science.1209038 (2011).
- 586 12 Kornmann, B. *et al.* An ER-mitochondria tethering complex revealed by a synthetic biology screen.  
587 *Science* **325**, 477-481, doi:10.1126/science.1175088 (2009).
- 588 13 Valm, A. M. *et al.* Applying systems-level spectral imaging and analysis to reveal the organelle  
589 interactome. *Nature* **546**, 162-167, doi:10.1038/nature22369 (2017).
- 590 14 Bohnert, M. Tether Me, Tether Me Not-Dynamic Organelle Contact Sites in Metabolic Rewiring. *Dev*  
591 *Cell* **54**, 212-225, doi:10.1016/j.devcel.2020.06.026 (2020).
- 592 15 Hansen, K. G. *et al.* An ER surface retrieval pathway safeguards the import of mitochondrial  
593 membrane proteins in yeast. *Science* **361**, 1118-1122, doi:10.1126/science.aar8174 (2018).
- 594 16 Carreras-Sureda, A. *et al.* Non-canonical function of IRE1alpha determines mitochondria-associated  
595 endoplasmic reticulum composition to control calcium transfer and bioenergetics. *Nat Cell Biol* **21**,  
596 755-767, doi:10.1038/s41556-019-0329-y (2019).
- 597 17 Bauerlein, F. J. B. *et al.* In Situ Architecture and Cellular Interactions of PolyQ Inclusions. *Cell* **171**,  
598 179-187 e110, doi:10.1016/j.cell.2017.08.009 (2017).
- 599 18 Hetz, C. & Mollereau, B. Disturbance of endoplasmic reticulum proteostasis in neurodegenerative  
600 diseases. *Nat Rev Neurosci* **15**, 233-249, doi:10.1038/nrn3689 (2014).
- 601 19 Boos, F., Labbadia, J. & Herrmann, J. M. How the Mitoprotein-Induced Stress Response Safeguards  
602 the Cytosol: A Unified View. *Trends Cell Biol* **30**, 241-254, doi:10.1016/j.tcb.2019.12.003 (2020).
- 603 20 Liu, Y. & Chang, A. Heat shock response relieves ER stress. *EMBO J* **27**, 1049-1059,  
604 doi:10.1038/emboj.2008.42 (2008).
- 605 21 Schmidt, R. M., Schessner, J. P., Borner, G. H. & Schuck, S. The proteasome biogenesis regulator  
606 Rpn4 cooperates with the unfolded protein response to promote ER stress resistance. *Elife* **8**,  
607 e43244, doi:10.7554/eLife.43244 (2019).
- 608 22 Lebeau, J. *et al.* The PERK Arm of the Unfolded Protein Response Regulates Mitochondrial  
609 Morphology during Acute Endoplasmic Reticulum Stress. *Cell Rep* **22**, 2827-2836,  
610 doi:10.1016/j.celrep.2018.02.055 (2018).

- 611 23 Pincus, D., Aranda-Diaz, A., Zuleta, I. A., Walter, P. & El-Samad, H. Delayed Ras/PKA signaling  
612 augments the unfolded protein response. *Proc Natl Acad Sci U S A* **111**, 14800-14805,  
613 doi:10.1073/pnas.1409588111 (2014).
- 614 24 Rolland, S. G. *et al.* Compromised Mitochondrial Protein Import Acts as a Signal for UPR(mt). *Cell*  
615 *Rep* **28**, 1659-1669 e1655, doi:10.1016/j.celrep.2019.07.049 (2019).
- 616 25 Nargund, A. M., Pellegrino, M. W., Fiorese, C. J., Baker, B. M. & Haynes, C. M. Mitochondrial import  
617 efficiency of ATFS-1 regulates mitochondrial UPR activation. *Science* **337**, 587-590,  
618 doi:10.1126/science.1223560 (2012).
- 619 26 Harbauer, A. B., Zahedi, R. P., Sickmann, A., Pfanner, N. & Meisinger, C. The protein import  
620 machinery of mitochondria-a regulatory hub in metabolism, stress, and disease. *Cell Metab* **19**,  
621 357-372, doi:10.1016/j.cmet.2014.01.010 (2014).
- 622 27 Wrobel, L. *et al.* Mistargeted mitochondrial proteins activate a proteostatic response in the cytosol.  
623 *Nature* **524**, 485-488, doi:10.1038/nature14951 (2015).
- 624 28 Boos, F. *et al.* Mitochondrial protein-induced stress triggers a global adaptive transcriptional  
625 programme. *Nat Cell Biol* **21**, 442-451, doi:10.1038/s41556-019-0294-5 (2019).
- 626 29 Kim, H. E. *et al.* Lipid Biosynthesis Coordinates a Mitochondrial-to-Cytosolic Stress Response. *Cell*  
627 **166**, 1539-1552 e1516, doi:10.1016/j.cell.2016.08.027 (2016).
- 628 30 Nargund, A. M., Fiorese, C. J., Pellegrino, M. W., Deng, P. & Haynes, C. M. Mitochondrial and  
629 nuclear accumulation of the transcription factor ATFS-1 promotes OXPHOS recovery during the  
630 UPR(mt). *Mol Cell* **58**, 123-133, doi:10.1016/j.molcel.2015.02.008 (2015).
- 631 31 Wang, X. & Chen, X. J. A cytosolic network suppressing mitochondria-mediated proteostatic stress  
632 and cell death. *Nature* **524**, 481-484, doi:10.1038/nature14859 (2015).
- 633 32 Fiorese, C. J. *et al.* The Transcription Factor ATF5 Mediates a Mammalian Mitochondrial UPR. *Curr*  
634 *Biol* **26**, 2037-2043, doi:10.1016/j.cub.2016.06.002 (2016).
- 635 33 Labbadia, J. *et al.* Mitochondrial Stress Restores the Heat Shock Response and Prevents  
636 Proteostasis Collapse during Aging. *Cell Rep* **21**, 1481-1494, doi:10.1016/j.celrep.2017.10.038  
637 (2017).
- 638 34 Guo, X. *et al.* Mitochondrial stress is relayed to the cytosol by an OMA1-DELE1-HRI pathway. *Nature*  
639 **579**, 427-432, doi:10.1038/s41586-020-2078-2 (2020).
- 640 35 Weidberg, H. & Amon, A. MitoCPR-A surveillance pathway that protects mitochondria in response  
641 to protein import stress. *Science* **360**, eaan4146, doi:10.1126/science.aan4146 (2018).
- 642 36 Mårtensson, C. U. *et al.* Mitochondrial protein translocation-associated degradation. *Nature* **569**,  
643 679-683, doi:10.1038/s41586-019-1227-y (2019).
- 644 37 Wienhues, U. *et al.* Protein folding causes an arrest of preprotein translocation into mitochondria in  
645 vivo. *J Cell Biol* **115**, 1601-1609, doi:10.1083/jcb.115.6.1601 (1991).
- 646 38 Rassow, J. *et al.* Translocation arrest by reversible folding of a precursor protein imported into  
647 mitochondria. A means to quantitate translocation contact sites. *J Cell Biol* **109**, 1421-1428,  
648 doi:10.1083/jcb.109.4.1421 (1989).
- 649 39 Eilers, M. & Schatz, G. Binding of a specific ligand inhibits import of a purified precursor protein into  
650 mitochondria. *Nature* **322**, 228-232, doi:10.1038/322228a0 (1986).
- 651 40 Samluk, L. *et al.* Cytosolic translational responses differ under conditions of severe short-term and  
652 long-term mitochondrial stress. *Mol Biol Cell* **30**, 1864-1877, doi:10.1091/mbc.E18-10-0628 (2019).
- 653 41 Tsaytler, P., Harding, H. P., Ron, D. & Bertolotti, A. Selective inhibition of a regulatory subunit of  
654 protein phosphatase 1 restores proteostasis. *Science* **332**, 91-94, doi:10.1126/science.1201396  
655 (2011).
- 656 42 Morimoto, R. I. Heat shock: the role of transient inducible responses in cell damage,  
657 transformation, and differentiation. *Cancer Cells* **3**, 295-301 (1991).
- 658 43 Mesecke, N. *et al.* A disulfide relay system in the intermembrane space of mitochondria that  
659 mediates protein import. *Cell* **121**, 1059-1069, doi:10.1016/j.cell.2005.04.011 (2005).
- 660 44 Chacinska, A. *et al.* Essential role of Mia40 in import and assembly of mitochondrial intermembrane  
661 space proteins. *EMBO J* **23**, 3735-3746, doi:10.1038/sj.emboj.7600389 (2004).
- 662 45 Weill, U. *et al.* Assessment of GFP Tag Position on Protein Localization and Growth Fitness in Yeast.  
663 *J Mol Biol* **431**, 636-641, doi:10.1016/j.jmb.2018.12.004 (2019).

- 664 46 Wigley, W. C., Stidham, R. D., Smith, N. M., Hunt, J. F. & Thomas, P. J. Protein solubility and folding  
665 monitored in vivo by structural complementation of a genetic marker protein. *Nat Biotechnol* **19**,  
666 131-136, doi:10.1038/84389 (2001).
- 667 47 Waldo, G. S., Standish, B. M., Berendzen, J. & Terwilliger, T. C. Rapid protein-folding assay using  
668 green fluorescent protein. *Nat Biotechnol* **17**, 691-695, doi:10.1038/10904 (1999).
- 669 48 Smoyer, C. J. *et al.* Analysis of membrane proteins localizing to the inner nuclear envelope in living  
670 cells. *J Cell Biol* **215**, 575-590, doi:10.1083/jcb.201607043 (2016).
- 671 49 Cabantous, S. & Waldo, G. S. In vivo and in vitro protein solubility assays using split GFP. *Nat*  
672 *Methods* **3**, 845-854, doi:10.1038/nmeth932 (2006).
- 673 50 Cabantous, S., Terwilliger, T. C. & Waldo, G. S. Protein tagging and detection with engineered self-  
674 assembling fragments of green fluorescent protein. *Nat Biotechnol* **23**, 102-107,  
675 doi:10.1038/nbt1044 (2005).
- 676 51 Pedelacq, J. D., Cabantous, S., Tran, T., Terwilliger, T. C. & Waldo, G. S. Engineering and  
677 characterization of a superfolder green fluorescent protein. *Nat Biotechnol* **24**, 79-88,  
678 doi:10.1038/nbt1172 (2006).
- 679 52 Wenz, L. S. *et al.* The presequence pathway is involved in protein sorting to the mitochondrial outer  
680 membrane. *EMBO Rep* **15**, 678-685, doi:10.1002/embr.201338144 (2014).
- 681 53 Song, J., Tamura, Y., Yoshihisa, T. & Endo, T. A novel import route for an N-anchor mitochondrial  
682 outer membrane protein aided by the TIM23 complex. *EMBO Rep* **15**, 670-677,  
683 doi:10.1002/embr.201338142 (2014).
- 684 54 Szyrach, G., Ott, M., Bonnefoy, N., Neupert, W. & Herrmann, J. M. Ribosome binding to the Oxa1  
685 complex facilitates co-translational protein insertion in mitochondria. *EMBO J* **22**, 6448-6457,  
686 doi:10.1093/emboj/cdg623 (2003).
- 687 55 Terziyska, N. *et al.* Mia40, a novel factor for protein import into the intermembrane space of  
688 mitochondria is able to bind metal ions. *FEBS Lett* **579**, 179-184, doi:10.1016/j.febslet.2004.11.072  
689 (2005).
- 690 56 Kater, L. *et al.* Structure of the Bcs1 AAA-ATPase suggests an airlock-like translocation mechanism  
691 for folded proteins. *Nat Struct Mol Biol* **27**, 142-149, doi:10.1038/s41594-019-0364-1 (2020).
- 692 57 Rojo, E. E., Guiard, B., Neupert, W. & Stuart, R. A. Sorting of D-lactate dehydrogenase to the inner  
693 membrane of mitochondria. Analysis of topogenic signal and energetic requirements. *J Biol Chem*  
694 **273**, 8040-8047, doi:10.1074/jbc.273.14.8040 (1998).
- 695 58 Wu, X., Cabanos, C. & Rapoport, T. A. Structure of the post-translational protein translocation  
696 machinery of the ER membrane. *Nature* **566**, 136-139, doi:10.1038/s41586-018-0856-x (2019).
- 697 59 Jan, C. H., Williams, C. C. & Weissman, J. S. Principles of ER cotranslational translocation revealed by  
698 proximity-specific ribosome profiling. *Science* **346**, 1257521, doi:10.1126/science.1257521 (2014).
- 699 60 Williams, C. C., Jan, C. H. & Weissman, J. S. Targeting and plasticity of mitochondrial proteins  
700 revealed by proximity-specific ribosome profiling. *Science* **346**, 748-751,  
701 doi:10.1126/science.1257522 (2014).
- 702 61 Fazal, F. M. *et al.* Atlas of Subcellular RNA Localization Revealed by APEX-Seq. *Cell* **178**, 473-490  
703 e426, doi:10.1016/j.cell.2019.05.027 (2019).
- 704 62 del Alamo, M. *et al.* Defining the specificity of cotranslationally acting chaperones by systematic  
705 analysis of mRNAs associated with ribosome-nascent chain complexes. *PLoS Biol* **9**, e1001100,  
706 doi:10.1371/journal.pbio.1001100 (2011).
- 707 63 Chartron, J. W., Hunt, K. C. & Frydman, J. Cotranslational signal-independent SRP preloading during  
708 membrane targeting. *Nature* **536**, 224-228, doi:10.1038/nature19309 (2016).
- 709 64 Ng, D. T., Brown, J. D. & Walter, P. Signal sequences specify the targeting route to the endoplasmic  
710 reticulum membrane. *J Cell Biol* **134**, 269-278, doi:10.1083/jcb.134.2.269 (1996).
- 711 65 Walter, P. & Blobel, G. Translocation of proteins across the endoplasmic reticulum III. Signal  
712 recognition protein (SRP) causes signal sequence-dependent and site-specific arrest of chain  
713 elongation that is released by microsomal membranes. *J Cell Biol* **91**, 557-561,  
714 doi:10.1083/jcb.91.2.557 (1981).
- 715 66 Costa, E. A., Subramanian, K., Nunnari, J. & Weissman, J. S. Defining the physiological role of SRP in  
716 protein-targeting efficiency and specificity. *Science* **359**, 689-692, doi:10.1126/science.aar3607  
717 (2018).

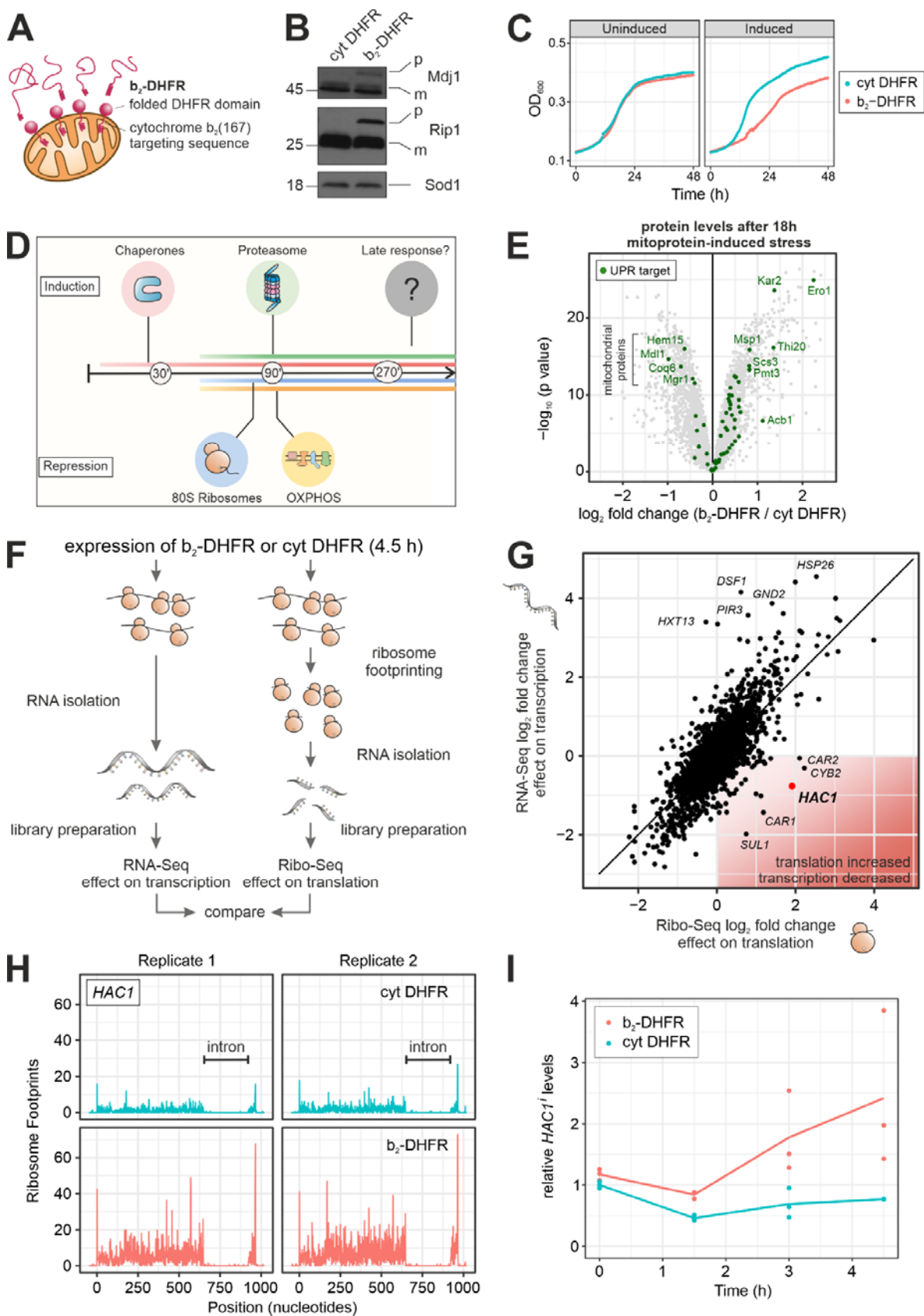
- 718 67 Wild, K., Halic, M., Sinning, I. & Beckmann, R. SRP meets the ribosome. *Nat Struct Mol Biol* **11**,  
719 1049-1053, doi:10.1038/nsmb853 (2004).
- 720 68 Paulo, J. A. *et al.* Quantitative mass spectrometry-based multiplexing compares the abundance of  
721 5000 *S. cerevisiae* proteins across 10 carbon sources. *J Proteomics* **148**, 85-93,  
722 doi:10.1016/j.jprot.2016.07.005 (2016).
- 723 69 Paulo, J. A., O'Connell, J. D., Gaun, A. & Gygi, S. P. Proteome-wide quantitative multiplexed profiling  
724 of protein expression: carbon-source dependency in *Saccharomyces cerevisiae*. *Mol Biol Cell* **26**,  
725 4063-4074, doi:10.1091/mbc.E15-07-0499 (2015).
- 726 70 Morgenstern, M. *et al.* Definition of a High-Confidence Mitochondrial Proteome at Quantitative  
727 Scale. *Cell Rep* **19**, 2836-2852, doi:10.1016/j.celrep.2017.06.014 (2017).
- 728 71 Di Bartolomeo, F. *et al.* Absolute yeast mitochondrial proteome quantification reveals trade-off  
729 between biosynthesis and energy generation during diauxic shift. *Proc Natl Acad Sci U S A* **117**,  
730 7524-7535, doi:10.1073/pnas.1918216117 (2020).
- 731 72 Murphy, J. P., Stepanova, E., Everley, R. A., Paulo, J. A. & Gygi, S. P. Comprehensive Temporal  
732 Protein Dynamics during the Diauxic Shift in *Saccharomyces cerevisiae*. *Mol Cell Proteomics* **14**,  
733 2454-2465, doi:10.1074/mcp.M114.045849 (2015).
- 734 73 Rubio, C. *et al.* Homeostatic adaptation to endoplasmic reticulum stress depends on Ire1 kinase  
735 activity. *J Cell Biol* **193**, 171-184, doi:10.1083/jcb.201007077 (2011).
- 736 74 Chawla, A., Chakrabarti, S., Ghosh, G. & Niwa, M. Attenuation of yeast UPR is essential for survival  
737 and is mediated by IRE1 kinase. *J Cell Biol* **193**, 41-50, doi:10.1083/jcb.201008071 (2011).
- 738 75 Shakya, V. P. *et al.* A nuclear-based quality control pathway for non-imported mitochondrial  
739 proteins. *Elife* **10**, doi:10.7554/eLife.61230 (2021).
- 740 76 Kowalski, L. *et al.* Determinants of the cytosolic turnover of mitochondrial intermembrane space  
741 proteins. *BMC Biol* **16**, 66, doi:10.1186/s12915-018-0536-1 (2018).
- 742 77 Nowicka, U. *et al.* Cytosolic aggregation of mitochondrial proteins disrupts cellular homeostasis by  
743 stimulating other proteins aggregation. *bioRxiv*, 2021.2005.2002.442342,  
744 doi:10.1101/2021.05.02.442342 (2021).
- 745 78 Liu, Y. *et al.* Mitochondrial carrier protein overloading and misfolding induce aggresomes and  
746 proteostatic adaptations in the cytosol. *Mol Biol Cell* **30**, 1272-1284, doi:10.1091/mbc.E19-01-0046  
747 (2019).
- 748 79 Backes, S. *et al.* The chaperone-binding activity of the mitochondrial surface receptor Tom70  
749 protects the cytosol against mitoprotein-induced stress. *Cell Rep* **35**, 108936,  
750 doi:10.1016/j.celrep.2021.108936 (2021).
- 751 80 Vincenz-Donnelly, L. *et al.* High capacity of the endoplasmic reticulum to prevent secretion and  
752 aggregation of amyloidogenic proteins. *EMBO J* **37**, 337-350, doi:10.15252/embj.201695841 (2018).
- 753 81 Rousseau, E. *et al.* Targeting expression of expanded polyglutamine proteins to the endoplasmic  
754 reticulum or mitochondria prevents their aggregation. *Proc Natl Acad Sci U S A* **101**, 9648-9653,  
755 doi:10.1073/pnas.0403015101 (2004).
- 756 82 Metzger, M. B., Maurer, M. J., Dancy, B. M. & Michaelis, S. Degradation of a cytosolic protein  
757 requires endoplasmic reticulum-associated degradation machinery. *J Biol Chem* **283**, 32302-32316,  
758 doi:10.1074/jbc.M806424200 (2008).
- 759 83 Laborenz, J. *et al.* The ER protein Ema19 facilitates the degradation of non-imported mitochondrial  
760 precursor proteins. *Mol Biol Cell*, mbcE20110748, doi:10.1091/mbc.E20-11-0748 (2021).
- 761 84 Tran, J. R., Tomsic, L. R. & Brodsky, J. L. A Cdc48p-associated factor modulates endoplasmic  
762 reticulum-associated degradation, cell stress, and ubiquitinated protein homeostasis. *J Biol Chem*  
763 **286**, 5744-5755, doi:10.1074/jbc.M110.179259 (2011).
- 764 85 Heo, J. M. *et al.* A stress-responsive system for mitochondrial protein degradation. *Mol Cell* **40**, 465-  
765 480, doi:10.1016/j.molcel.2010.10.021 (2010).
- 766 86 Caplan, A. J., Cyr, D. M. & Douglas, M. G. YDJ1p facilitates polypeptide translocation across different  
767 intracellular membranes by a conserved mechanism. *Cell* **71**, 1143-1155, doi:10.1016/s0092-  
768 8674(05)80063-7 (1992).
- 769 87 Opaliński, Ł. *et al.* Recruitment of Cytosolic J-Proteins by TOM Receptors Promotes Mitochondrial  
770 Protein Biogenesis. *Cell Rep* **25**, 2036-2043 e2035, doi:10.1016/j.celrep.2018.10.083 (2018).

- 771 88 Xiao, T., Shakya, V. P. & Hughes, A. L. ER targeting of non-imported mitochondrial carrier proteins is  
772 dependent on the GET pathway. *Life Sci Alliance* **4**, doi:10.26508/lsa.202000918 (2021).
- 773 89 Matsumoto, S. *et al.* Msp1 Clears Mistargeted Proteins by Facilitating Their Transfer from  
774 Mitochondria to the ER. *Mol Cell* **76**, 191-205 e110, doi:10.1016/j.molcel.2019.07.006 (2019).
- 775 90 Dederer, V. *et al.* Cooperation of mitochondrial and ER factors in quality control of tail-anchored  
776 proteins. *Elife* **8**, doi:10.7554/eLife.45506 (2019).
- 777 91 McKenna, M. J. *et al.* The endoplasmic reticulum P5A-ATPase is a transmembrane helix dislocase.  
778 *Science* **369**, doi:10.1126/science.abc5809 (2020).
- 779 92 Hayashi, T., Rizzuto, R., Hajnoczky, G. & Su, T. P. MAM: more than just a housekeeper. *Trends Cell*  
780 *Biol* **19**, 81-88, doi:10.1016/j.tcb.2008.12.002 (2009).
- 781 93 Munoz, J. P. *et al.* Mfn2 modulates the UPR and mitochondrial function via repression of PERK.  
782 *EMBO J* **32**, 2348-2361, doi:10.1038/emboj.2013.168 (2013).
- 783 94 Böckler, S. & Westermann, B. Mitochondrial ER contacts are crucial for mitophagy in yeast. *Dev Cell*  
784 **28**, 450-458, doi:10.1016/j.devcel.2014.01.012 (2014).
- 785 95 Hamasaki, M. *et al.* Autophagosomes form at ER-mitochondria contact sites. *Nature* **495**, 389-393,  
786 doi:10.1038/nature11910 (2013).
- 787 96 Vitali, D. G. *et al.* The GET pathway can increase the risk of mitochondrial outer membrane proteins  
788 to be mistargeted to the ER. *J Cell Sci* **131**, doi:10.1242/jcs.211110 (2018).
- 789 97 Rainbolt, T. K., Saunders, J. M. & Wiseman, R. L. Stress-responsive regulation of mitochondria  
790 through the ER unfolded protein response. *Trends Endocrinol Metab* **25**, 528-537,  
791 doi:10.1016/j.tem.2014.06.007 (2014).
- 792 98 Eiyama, A., Aaltonen, M. J., Nolte, H., Tatsuta, T. & Langer, T. Disturbed intramitochondrial  
793 phosphatidic acid transport impairs cellular stress signaling. *J Biol Chem*, 100335,  
794 doi:10.1016/j.jbc.2021.100335 (2021).
- 795 99 Tran, D. M., Ishiwata-Kimata, Y., Mai, T. C., Kubo, M. & Kimata, Y. The unfolded protein response  
796 alongside the diauxic shift of yeast cells and its involvement in mitochondria enlargement. *Sci Rep*  
797 **9**, 12780, doi:10.1038/s41598-019-49146-5 (2019).
- 798 100 Yong, J. *et al.* Mitochondria supply ATP to the ER through a mechanism antagonized by cytosolic  
799 Ca<sup>2+</sup>. *Elife* **8**, doi:10.7554/eLife.49682 (2019).
- 800 101 Costa, R. *et al.* Impaired Mitochondrial ATP Production Downregulates Wnt Signaling via ER Stress  
801 Induction. *Cell Rep* **28**, 1949-1960 e1946, doi:10.1016/j.celrep.2019.07.050 (2019).
- 802 102 Balsa, E. *et al.* ER and Nutrient Stress Promote Assembly of Respiratory Chain Supercomplexes  
803 through the PERK-eIF2alpha Axis. *Mol Cell* **74**, 877-890 e876, doi:10.1016/j.molcel.2019.03.031  
804 (2019).
- 805 103 Sikorski, R. S. & Hieter, P. A system of shuttle vectors and yeast host strains designed for efficient  
806 manipulation of DNA in *Saccharomyces cerevisiae*. *Genetics* **122**, 19-27 (1989).
- 807 104 Thomas, B. J. & Rothstein, R. Elevated recombination rates in transcriptionally active DNA. *Cell* **56**,  
808 619-630, doi:10.1016/0092-8674(89)90584-9 (1989).
- 809 105 Botman, D., de Groot, D. H., Schmidt, P., Goedhart, J. & Teusink, B. In vivo characterisation of  
810 fluorescent proteins in budding yeast. *Sci Rep* **9**, 2234, doi:10.1038/s41598-019-38913-z (2019).
- 811 106 Janke, C. *et al.* A versatile toolbox for PCR-based tagging of yeast genes: new fluorescent proteins,  
812 more markers and promoter substitution cassettes. *Yeast* **21**, 947-962, doi:10.1002/yea.1142  
813 (2004).
- 814 107 Livak, K. J. & Schmittgen, T. D. Analysis of relative gene expression data using real-time quantitative  
815 PCR and the 2<sup>-</sup>(Delta Delta C(T)) Method. *Methods* **25**, 402-408, doi:10.1006/meth.2001.1262  
816 (2001).
- 817 108 Ingolia, N. T., Brar, G. A., Rouskin, S., McGeachy, A. M. & Weissman, J. S. The ribosome profiling  
818 strategy for monitoring translation in vivo by deep sequencing of ribosome-protected mRNA  
819 fragments. *Nat Protoc* **7**, 1534-1550, doi:10.1038/nprot.2012.086 (2012).
- 820 109 Langmead, B., Trapnell, C., Pop, M. & Salzberg, S. L. Ultrafast and memory-efficient alignment of  
821 short DNA sequences to the human genome. *Genome Biol* **10**, R25, doi:10.1186/gb-2009-10-3-r25  
822 (2009).
- 823 110 Anders, S., Pyl, P. T. & Huber, W. HTSeq--a Python framework to work with high-throughput  
824 sequencing data. *Bioinformatics* **31**, 166-169, doi:10.1093/bioinformatics/btu638 (2015).

825 111 Love, M. I., Huber, W. & Anders, S. Moderated estimation of fold change and dispersion for RNA-  
826 seq data with DESeq2. *Genome Biol* **15**, 550, doi:10.1186/s13059-014-0550-8 (2014).  
827 112 Huber, W. *et al.* Orchestrating high-throughput genomic analysis with Bioconductor. *Nat Methods*  
828 **12**, 115-121, doi:10.1038/nmeth.3252 (2015).  
829 113 Rath, S. *et al.* MitoCarta3.0: an updated mitochondrial proteome now with sub-organelle  
830 localization and pathway annotations. *Nucleic Acids Res* **49**, D1541-D1547,  
831 doi:10.1093/nar/gkaa1011 (2021).  
832 114 Barrett, T. *et al.* NCBI GEO: archive for functional genomics data sets--update. *Nucleic Acids Res* **41**,  
833 D991-995, doi:10.1093/nar/gks1193 (2013).  
834

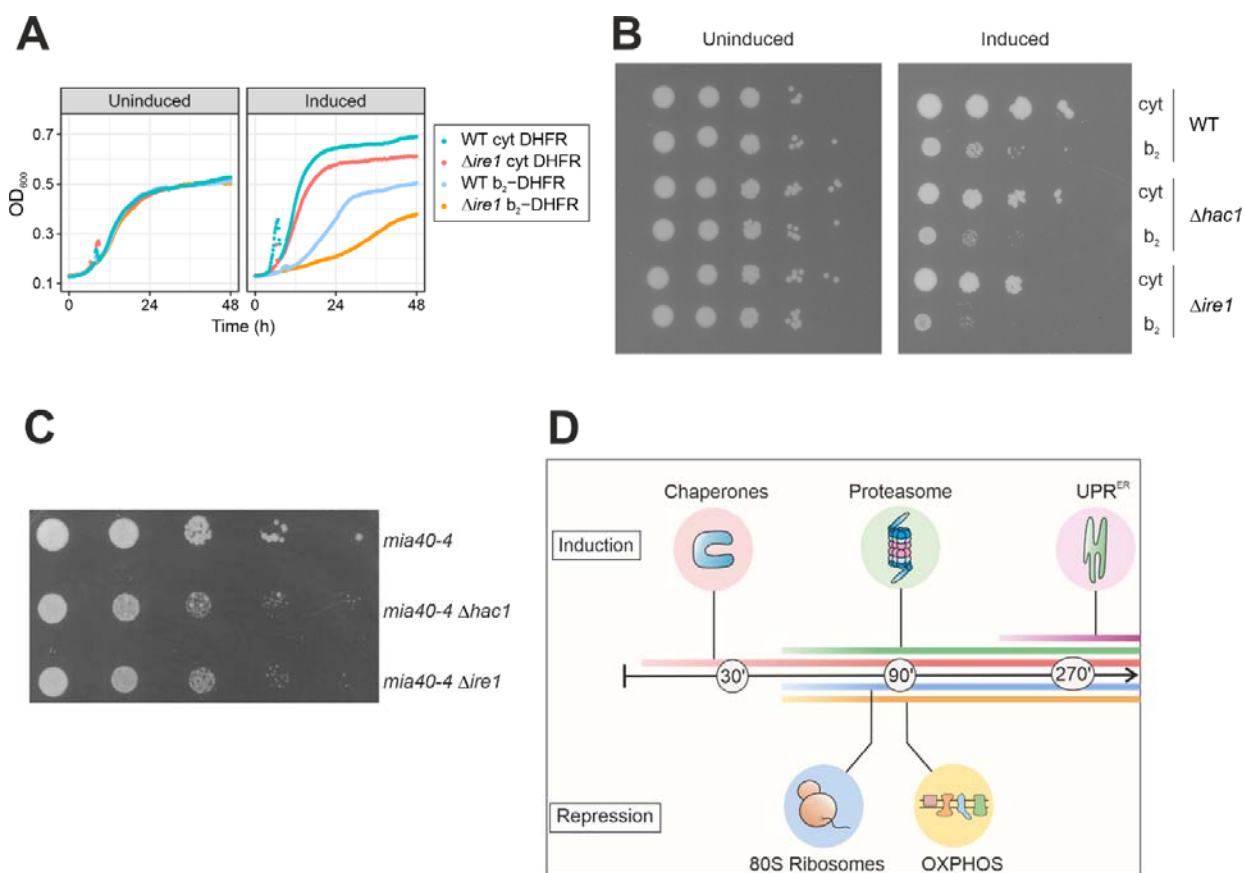


835 **Figures and Figure Legends**



837 **Figure 1. Mitoprotein-induced stress triggers the UPR<sup>ER</sup>.** **A**, Fusion of DHFR to the N-terminus  
838 of Cytochrome *b<sub>2</sub>* generates a mitochondrial ‘clogger’ that jams the protein import machinery. **B**,  
839 The mitochondrial clogger *b<sub>2</sub>*-DHFR or cytosolic DHFR were expressed for 4.5 h. The precursor  
840 form of the mitochondrial proteins Mdj1 and Rip1 were detected by Western Blotting. **C**,  
841 Expression of *b<sub>2</sub>*-DHFR leads to attenuated growth. **D**, The mitoprotein-induced stress response  
842 encompasses an early transcriptional induction of chaperones and the proteasome and a  
843 downregulation of cytosolic ribosomes and OXPHOS components. **E**, Protein levels in clogger-  
844 expressing versus control cells after 18 h of induction were measured by quantitative mass  
845 spectrometry<sup>28</sup>. Highlighted are proteins which are reported targets of the UPR<sup>ER</sup><sup>21</sup>. Data from *n*=3  
846 independent biological replicates are shown. **F**, **G**, The cellular transcriptome and translome after  
847 4.5 h of clogger induction were measured by RNA-Seq (*n*=4)<sup>28</sup> and ribosome profiling (*n*=3),  
848 respectively. Shown are log<sub>2</sub> fold changes of *b<sub>2</sub>*-DHFR versus cytosolic DHFR. *HAC1* transcripts  
849 are slightly reduced, but its translation is upregulated. **H**, Ribosome footprints along the *HAC1* gene  
850 from cells expressing *b<sub>2</sub>*-DHFR or cytosolic DHFR for 4.5 h are shown. **I**, Levels of spliced *HAC1*  
851 mRNA in cells expressing *b<sub>2</sub>*-DHFR or cytosolic DHFR were measured by RT-qPCR over time  
852 (*n*=3).

853



854

855 **Figure 2. The UPR<sup>ER</sup> is required for cellular fitness under mitoprotein-induced stress**

856 **conditions.** **A**, Wild type and *Δire1* cells were grown under non-inducing (left) or inducing (right)

857 conditions, expressing either *b<sub>2</sub>*-DHFR or cytosolic DHFR. *Δire1* cells are more susceptible to

858 mitoprotein-induced stress. **B**, Tenfold serial dilutions of wild type, *Δire1* and *Δhac1* cultures were

859 dropped on lactate plates with ('induced) or without ('uninduced') 0.5% galactose. The UPR<sup>ER</sup>-

860 deficient mutants show synthetic growth defects with expression of *b<sub>2</sub>*-DHFR. **C**, *HAC1* and *IRE1*

861 were deleted in temperature-sensitive *mia40-4* mutants. Cells were grown in glucose medium and

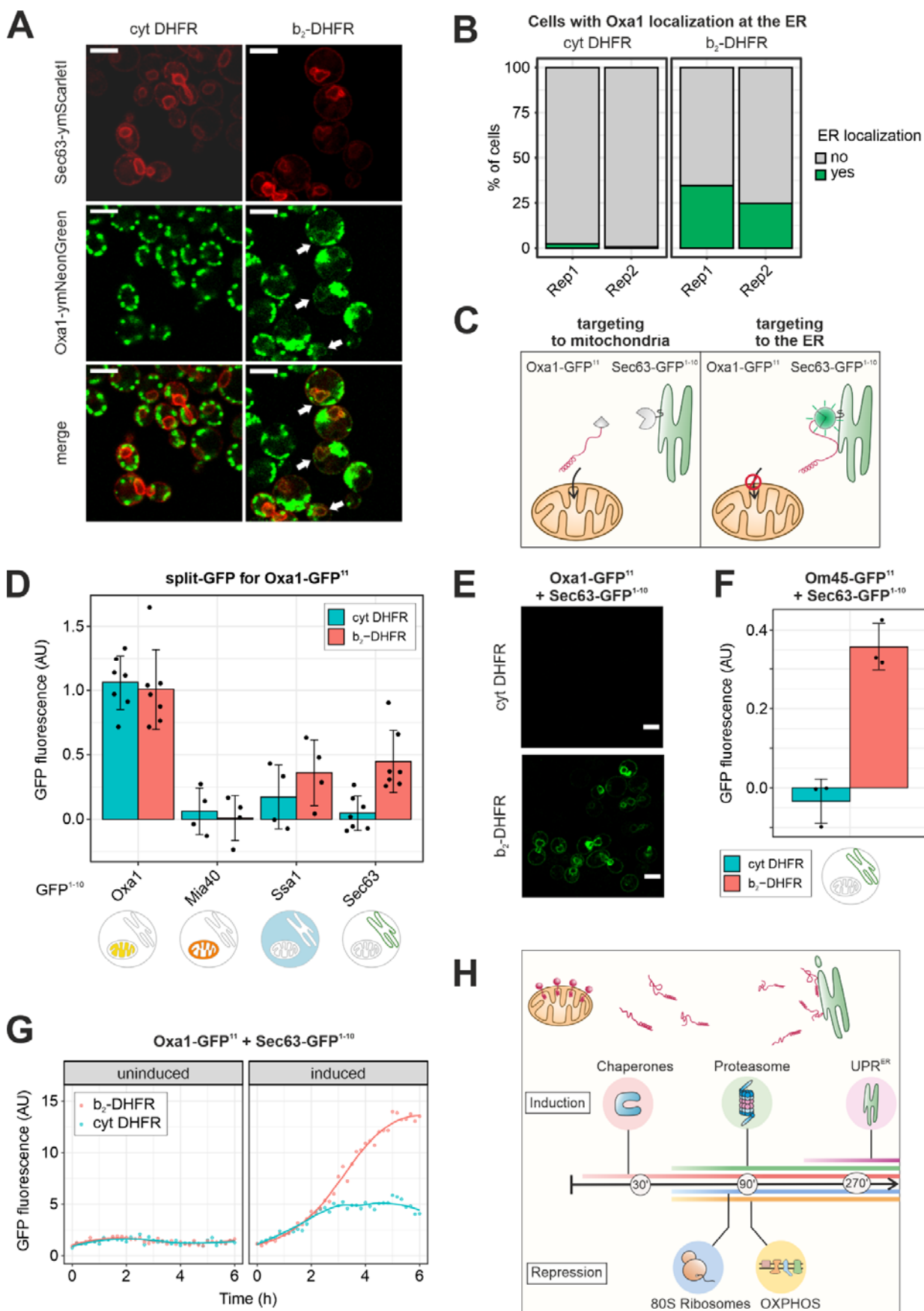
862 serial dilutions were spotted on glucose plates and incubated at the semi-permissive temperature of

863 30°C. Loss of the UPR<sup>ER</sup> results in synthetic growth defects. **D**, Early cytonuclear adaptations to

864 mitoprotein-induced stress are accompanied by the induction of the UPR<sup>ER</sup> as a second line of

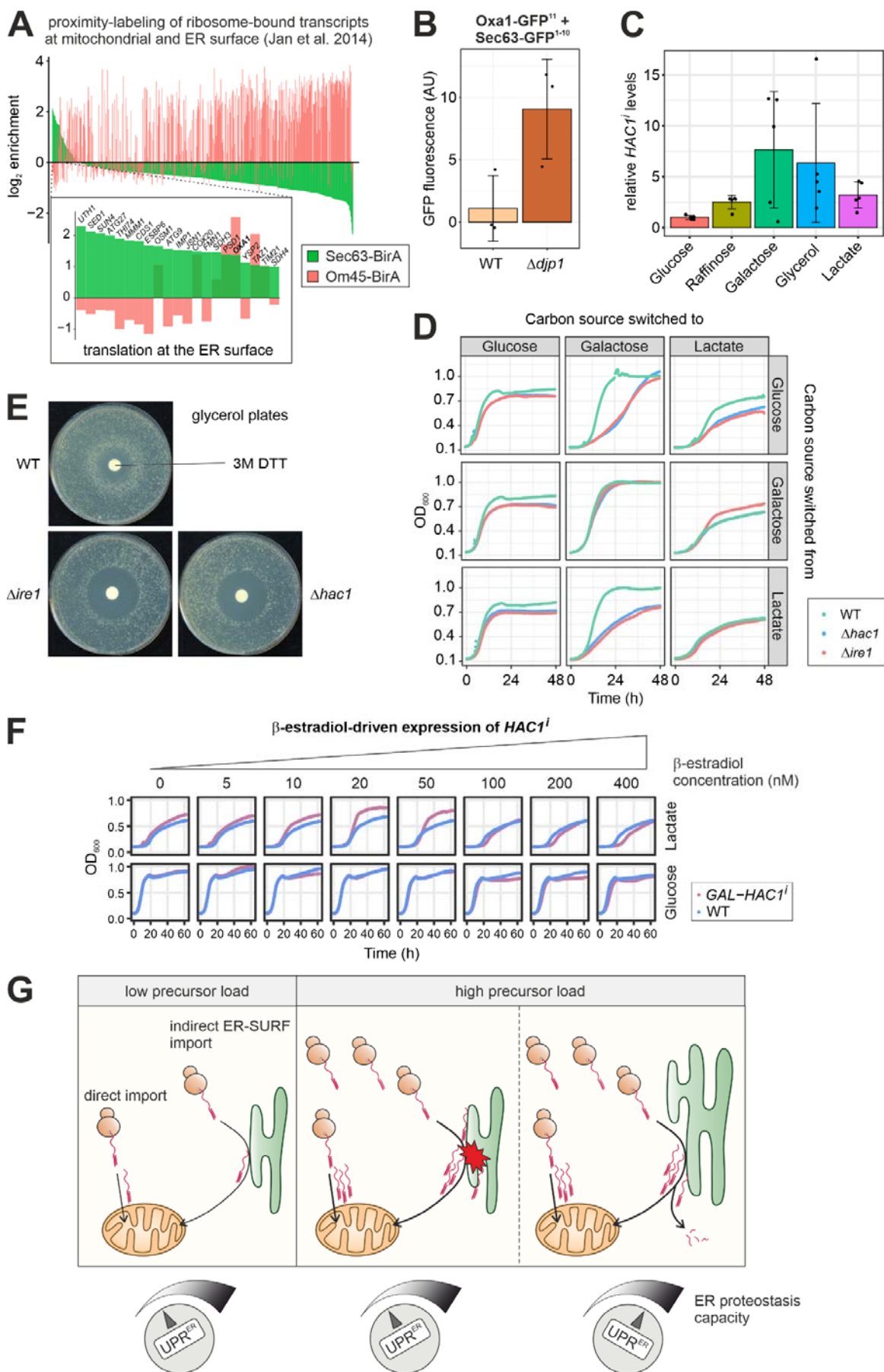
865 defense.

866



868 **Figure 3. Non-imported mitochondrial membrane proteins localize to the ER. A,** The  
869 mitochondrial inner membrane protein Oxa1 was genomically tagged with ymNeonGreen, the ER  
870 marker Sec63 was tagged with ymScarletI. Confocal fluorescence microscopy was performed after  
871 4.5 h of expression of either *b*<sub>2</sub>-DHFR or cytosolic DHFR. When the clogger was induced, a  
872 fraction of Oxa1-ymNeonGreen colocalized with Sec63-ymScarletI. Scale bar, 5 μm. **B,**  
873 Quantification of the number of cells from A in which ER localization of Oxa1-ymNeonGreen was  
874 observed. **C,** Schematic depiction of the split-GFP strategy to measure ER localization of  
875 mitochondrial proteins. **D,** The GFP<sup>11</sup> fragment was fused to Oxa1 and the GFP<sup>1-10</sup> fragment was  
876 fused to Oxa1, Mia40, Ssa1 or Sec63. *b*<sub>2</sub>-DHFR or cytosolic DHFR were induced for 4.5 h and  
877 fluorescence was measured in a platerreader. Mean values and standard deviations are shown for  
878 *n*=7 (Oxa1-GFP<sup>1-10</sup>, Sec63-GFP<sup>1-10</sup>) or *n*=4 (Mia40-GFP<sup>1-10</sup>, Ssa1-GFP<sup>1-10</sup>) independent biological  
879 replicates. **E,** Fluorescence microscopy of cells expressing Oxa1-GFP<sup>11</sup> and Sec63-GFP<sup>1-10</sup> and  
880 either *b*<sub>2</sub>-DHFR or cytosolic DHFR after 4.5 h of induction. Scale bar, 5 μm. **F,** The GFP<sup>11</sup>  
881 fragment was fused to Om45 and the GFP<sup>1-10</sup> fragment to Sec63. Clogger expression for 4.5 h  
882 evoked an increase in fluorescence (mean values and standard deviations for *n*=3 independent  
883 biological replicates). **G,** Cells expressing Oxa1-GFP<sup>11</sup> and Sec63-GFP<sup>1-10</sup> were cultured in lactate  
884 medium before either *b*<sub>2</sub>-DHFR or cytosolic DHFR were induced by addition of 0.5 % galactose.  
885 Fluorescence was monitored in a Clariostar plate reader every 10 min for *n*=6 biological replicates.  
886 Constitutively expressed ymScarletI was used to normalize for growth and overall translation rates.  
887 After around 3 h of induction, elevated split-GFP signals in clogger-expressing cells indicated  
888 accumulation of Oxa1 at the ER. **H,** Model for the connection between mitochondrial import block  
889 and UPR<sup>ER</sup> induction. Clogging the mitochondrial translocases leads to accumulation of precursor  
890 proteins in the cytosol as well as at the ER surface, which triggers the ER stress response.

891





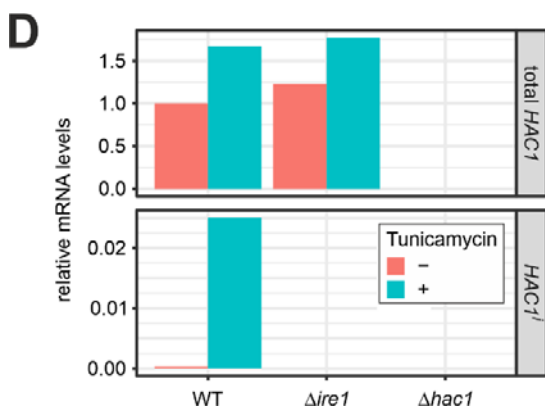
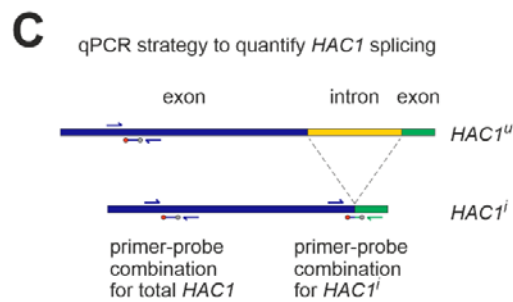
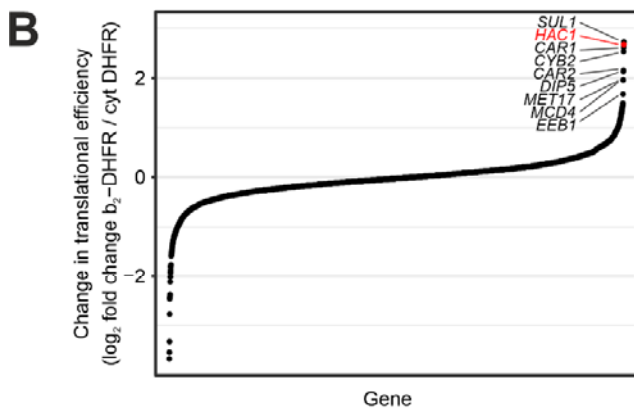
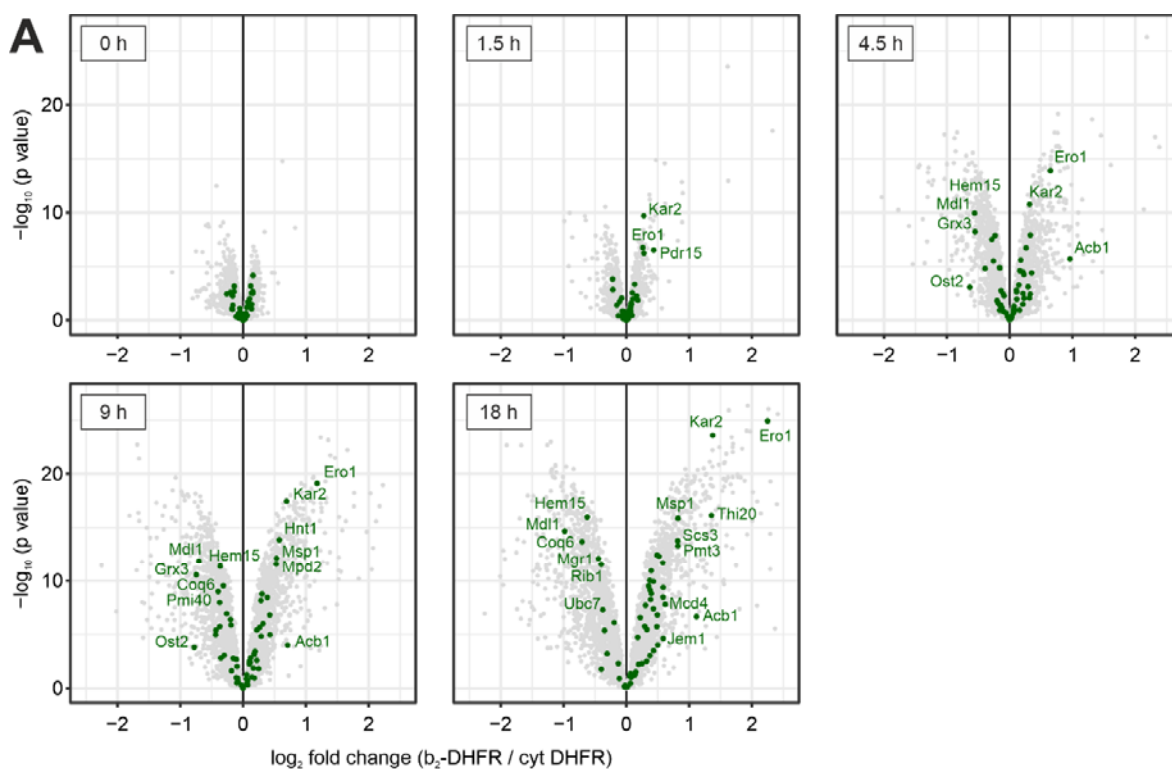
893 **Figure 4. The UPR<sup>ER</sup> maintains cellular fitness during changes in mitochondrial biogenesis. A,**  
894 Data from Jan et al. (2014)<sup>59</sup> on the localized translation near the mitochondrial and the ER surface.  
895 For all mitochondrial proteins in the dataset, the log<sub>2</sub> enrichment of ribosome-nascent chain  
896 complexes at the ER membrane (Sec63-BirA) and the mitochondrial outer membrane (Om45-BirA)  
897 over the total ribosomes are shown. While most translated mRNAs localize to the mitochondrial  
898 membrane, some transcripts are also or even exclusively enriched near the ER surface (expansion  
899 shows genes with more than 2-fold enrichment at the ER). **B,** The ER localization of Oxa1 was  
900 determined with the split-GFP assay in wild type and  $\Delta djp1$  cells that were grown to log phase in  
901 glucose medium. Oxa1 is trapped at the ER in  $\Delta djp1$ . Mean values and standard deviations from  
902  $n=3$  independent biological replicates are shown. **C,** *HAC1* splicing in wild type cells grown to log  
903 phase in media with the indicated carbon sources was measured via RT-qPCR. *HAC1<sup>i</sup>* levels were  
904 normalized to total *HAC1* levels. Mean values and standard deviations from  $n=5$  independent  
905 biological replicates are shown. **D,** Wild type,  $\Delta ire1$  and  $\Delta hac1$  cells were grown to log phase in  
906 glucose, galactose and lactate media, washed and switched to glucose, galactose and lactate media  
907 in all combinations. Growth was monitored by OD<sub>600</sub> measurement in a plate reader. Both UPR<sup>ER</sup>-  
908 deficient mutants showed impaired growth when the carbon source was switched to one that  
909 promotes higher levels of *HAC1* splicing in wild type cells. **E,** Wild type,  $\Delta ire1$  and  $\Delta hac1$  cells  
910 were plated on glycerol and 10  $\mu$ l of a 3 M solution of the UPR<sup>ER</sup>-inducing agent dithiothreitol  
911 (DTT) were applied on a filter dish in the middle of the plate. Note the ring-like growth of the wild  
912 type around the filter dish. **F,** Wild type cells and cells that express *HAC1<sup>i</sup>* from an estradiol-  
913 inducible *GAL* promoter were grown to log phase in glucose medium. They were washed,  
914 resuspended in either glucose or lactate medium supplemented with the indicated concentration of  
915 estradiol. Ectopic expression of low levels of *HAC1<sup>i</sup>* result in better growth in lactate, but not in  
916 glucose medium. **G,** Schematic model for the role of the UPR<sup>ER</sup> in mitochondrial protein  
917 biogenesis. A fraction of mitochondrial precursor proteins constantly localizes to the ER. Global  
918 changes in expression of mitochondrial genes increase the influx of precursors to the ER. Defects in

919 protein import also elevate the levels of ER-resident mitochondrial precursors. In both cases,  
920 activation of the UPR<sup>ER</sup> adjusts the proteostasis capacity of the ER.

921



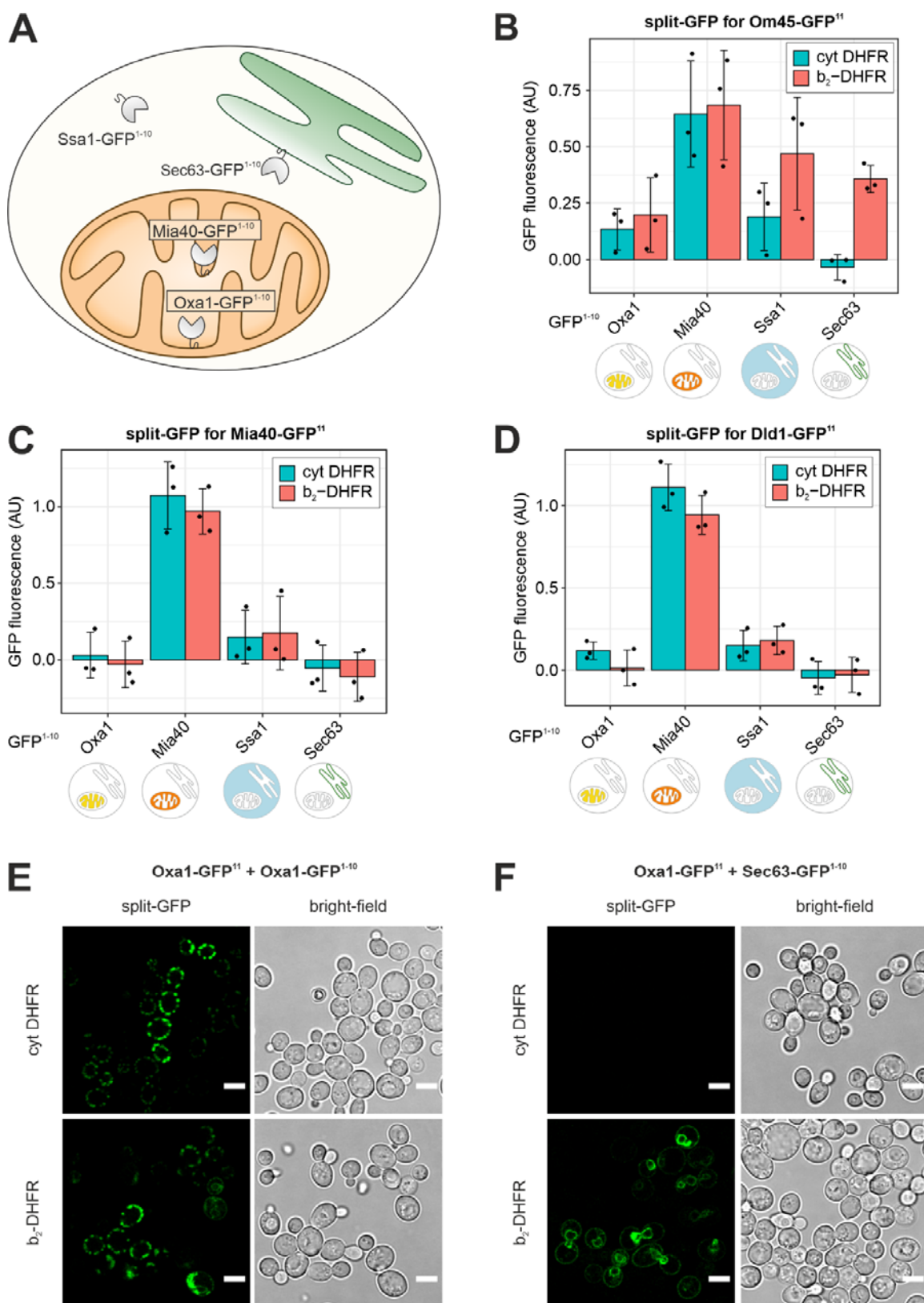
922 **Supplementary Figures**



924 **Supplementary Figure 1. Detection of UPR<sup>ER</sup> induction with mass spectrometry and RT-**  
925 **qPCR.**

926 **A**, Protein levels in clogger-expressing versus control cells after different times of induction were  
927 measured by quantitative mass spectrometry<sup>28</sup>. Highlighted are proteins which are reported targets  
928 of the UPR<sup>ER</sup><sup>21</sup>. Data from  $n=3$  independent biological replicates are shown. The data for 18 h are  
929 the same as shown in Fig. 1E. **B**, The change in translational efficiency after 4.5 h clogger  
930 expression was calculated for all genes measured in both the RNA-seq<sup>28</sup> and Ribo-Seq on clogger-  
931 expressing cells by dividing the translome fold change by the transcriptome fold change. **C**,  
932 Schematic depiction of the primer-probe combinations used to quantify total *HAC1* as well as  
933 spliced *HAC1<sup>i</sup>* mRNA levels via RT-qPCR. **D**, Wild type,  $\Delta ire1$  and  $\Delta hac1$  cells were grown in  
934 presence or absence of 1  $\mu\text{g/ml}$  tunicamycin and *HAC1* and *HAC1<sup>i</sup>* levels were analyzed with the  
935 primer-probe assay shown in C. As expected, *HAC1<sup>i</sup>* levels increased in wild type cells treated with  
936 tunicamycin, but no *HAC1<sup>i</sup>* was detected in cells lacking *HAC1* or *IRE1*, confirming the specificity  
937 of the RT-qPCR assay.

938



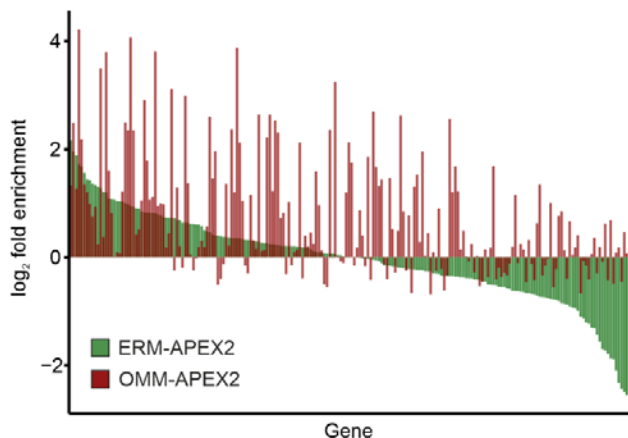
939

940 **Supplementary Figure 2. A split-GFP assay to assess the subcellular localization of**  
 941 **mitochondrial precursor proteins. A, The GFP<sup>11</sup> fragment was fused to Oxa1, Om45, Mia40 and**

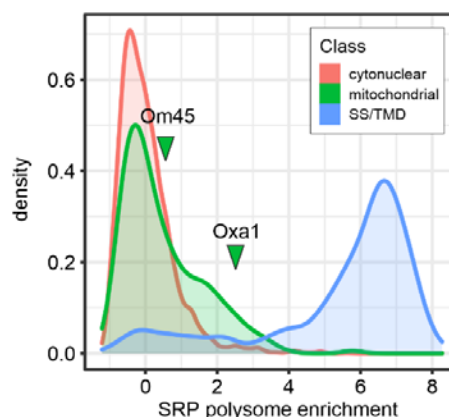
942 Dld1, and the GFP<sup>1-10</sup> reporter was fused to Oxa1 (mitochondrial inner membrane, matrix side),  
943 Mia40 (mitochondrial inner membrane, IMS side), Sec63 (ER membrane, cytosolic side) and Ssa1  
944 (cytosol). **B-D**, The split-GFP constructs described in A were co-expressed with *b*<sub>2</sub>-DHFR or  
945 cytosolic DHFR and fluorescence was measured with a Clariostar plate reader. Under non-stressed  
946 conditions (expression of cytosolic DHFR), the split-GFP signals recapitulated the known  
947 localizations of Oxa1, Om45, Mia40 and Dld1. Under mitoprotein-induced stress (*b*<sub>2</sub>-DHFR  
948 expression), Om45-GFP<sup>11</sup> also evoked a fluorescence signal when combined with Sec63-GFP<sup>1-10</sup>  
949 and Ssa1-GFP<sup>1-10</sup>, indicating accumulation at the cytosolic side of the ER membrane. **E**,  
950 Fluorescence microscopy of cells expressing Oxa1-GFP<sup>11</sup> and Oxa1-GFP<sup>1-10</sup> and either *b*<sub>2</sub>-DHFR or  
951 cytosolic DHFR after 4.5 h of induction. Scale bar, 5 μm. **F**, Fluorescence microscopy of cells  
952 expressing Oxa1-GFP<sup>11</sup> and Sec63-GFP<sup>1-10</sup> and either *b*<sub>2</sub>-DHFR or cytosolic DHFR after 4.5 h of  
953 induction. Scale bar, 5 μm. GFP Images are identical to those in Figure 3E.

954

**A** proximity-labeling of transcripts in HEK293T cells at mitochondrial and ER surface (Fazal et al. 2019)



**B** ribosome profiling of SRP-bound polysomes (Chartron et al. 2016)



955

956 **Supplementary Figure 3. Certain mitochondrial proteins are synthesized close to the ER**

957 **surface and recognized by SRP. A**, Data from Fazal et al. (2019)<sup>61</sup> on the subcellular distribution

958 of mRNA in HEK293T cells. The biotin ligase APEX2 was localized to the ER or mitochondria and

959 biotinylated mRNAs were purified and sequenced (APEX-Seq). For all mitochondrial proteins in

960 the dataset, the log<sub>2</sub> enrichment of mRNAs at the ER membrane (ERM-APEX2) and the

961 mitochondrial outer membrane (OMM-APEX2) over the total mRNAs are shown. While most

962 mRNAs localize to the mitochondrial membrane, some transcripts are also enriched near the ER

963 surface. **B**, Data from Chartron et al. (2016)<sup>63</sup> on the SRP-bound translato

964 me in yeast. SRP was immune-purified from cell lysates and the co-isolated ribosome-nascent chains complexes were

965 analyzed by ribosome profiling. The distribution of the log<sub>2</sub> fold enrichment SRP-bound ribosome-

966 nascent chain complexes over total ribosomes is shown for cytonuclear and mitochondrial proteins

967 and proteins that carry a signal sequence or transmembrane domain for ER targeting (SS/TMD).

968 Some mitochondrial proteins, including Oxa1, are bound by SRP.

969 **Supplementary Tables**

970 **Supplementary Table 1.** Yeast strains used in this study.

971 **Supplementary Table 2.** Plasmids used in this study.

972 **Supplementary Table 3.** Primers used in this study.